# Evaluation of singular and hypersingular Galerkin integrals: direct limits and symbolic computation

L. J. Gray
*Computer Science and Mathematics Division*
*Oak Ridge National Laboratory, Oak Ridge, TN 37831, USA*
*EMail: ljg@ornl.gov*

## Abstract

Algorithms are presented for evaluating singular and hypersingular boundary integrals arising from a Galerkin approximation in two dimensions. The integrals involving derivatives of the Green's function are defined as limits from the interior, allowing a simple and direct treatment of these terms. An efficient scheme is obtained by using a combined analytical and numerical approach, the analytic formulas easily derived with a symbolic computation program. The analytic integration also permits exact cancellation of potentially divergent terms, and thus the method is accurate as well. These algorithms are first presented in the simplest context, a linear element. The integrals resulting from higher order curved interpolation are shown to be reducible to the linear case, and can therefore be treated with the same techniques. Example calculations employing the Symmetric-Galerkin approximation are presented for the Laplace equation and for orthotropic elasticity. The post-processing evaluation of surface tangential derivatives is also discussed. These methods are applied to the modeling of void movement in the aluminum thin film interconnects employed in micro-electronics.

## 1 Introduction

Despite the fact that the Galerkin boundary integral method is a mathematically well studied technique, Schatz *et al.* [1], a perusal of engineering oriented texts, *e.g.*, Banerjee [2], Becker [3], Brebbia *et al.* [4], Kane [5], or, for that matter the present volume, clearly indicates that *collocation* is the dominant approximation in applications. The Galerkin procedure employs an additional boundary integration, and has therefore been a more complicated and a significantly slower method than collocation. However, two important and related advancements have radically altered this situation. The first is the emergence of hypersingular equations

as an essential tool in boundary integral analysis [6], in particular for the many important applications involving a crack geometry [7, 8, 9]. The Galerkin double integration effectively mollifies the hypersingular integral, and thereby simplifies the computation, whereas a collocation approximation must deal with a difficult numerical constraint, smooth interpolation of the coefficient function – referred to here as the $C^1$ condition. The second critical innovation is the development of the Symmetric-Galerkin method [10, 11, 12]. The symmetry can be exploited to produce a *fast* Galerkin algorithm, and this eliminates the dramatic advantage in computation time previously enjoyed by collocation [13].

The first numerical work employing hypersingular equations was likely in connection with linear elastic fracture analysis [14, 15], and hypersingular methods – *dual equations* [16, 17, 18, 19] or *displacement discontinity* [14, 20, 21, 22] – now dominate this subject [23]. Although special purpose, non-hypersingular, fracture algorithms have been devised for elasticity [24, 25], it appears that an effective general technique for a crack geometry must involve hypersingular equations. This application alone makes the ability to work with hypersingular equations absolutely essential.

Hypersingular integrals can be converted to a numerically tractable form by a variety of methods [26-32], and several reviews of this area are available [6, 33, 34]. Nevertheless, evaluation with collocation remains a difficult proposition. A physically sensible definition of the integral requires *differentiability* of the coefficient function, *e.g.*, potential for the Laplace equation, displacement in elasticity, at the collocation point [35, 36, 37] – more precisely, the function must have a Hölder continuous first derivative, $C^{1,\alpha}$. There has been considerable discussion of this point in the recent literature [42-45] (a good indication that collocating hypersingular integrals is not an easy matter!), and Section 3 will also consider this issue. For collocation, either a smooth interpolation, such as Overhauser [42, 43, 44, 45] or Hermite [46, 47, 48] elements, or a non-conforming (discontinuous) approximation [49, 50] must be employed. These techniques work reasonably well in two dimensions, but are much less attractive for three dimensional problems. The implementation for Overhauser cubic splines is complicated and oscillations can occur in the interpolation over non-uniform grids. The Hermite approach is expensive, involving simultaneous solution of the nodal tangential derivatives, and the application to fracture problems is not straightforward [46, 51]. The drawback associated with a non-conforming approximation, aside from the physically unappealing discontinuous nature of the approximation, is a significant increase in computational expense. The number of unknowns is much larger than with a corresponding conforming element, especially for three dimensional vector problems.

In the Galerkin approach, however, there is no smoothness constraint associated with hypersingular evaluation. The intuitive argument is that the second boundary integration effectively negates the differentiation creating the hypersingular kernel, and thus the resulting integral is effectively no worse than the 'Cauchy Principal Value' (CPV) integral in collocation. A more convincing argument is to evaluate the integral directly and show that it has a finite value, as will be carried out in Section 4. Hypersingular integrals can therefore be evaluated using standard continuous elements, and in this respect, Galerkin becomes

a simpler method than collocation. It will be argued herein that the evaluation of the singular integrals, probably perceived as a major complication of the Galerkin approach, is not especially difficult. This evaluation can be easily carried out by taking advantage of the analytic integration capabilities of a symbolic computation program such as Maple [52]. This permits a direct hybrid analytical/numerical singular integration approach which is completely general and, moreover, produces highly efficient algorithms [13].

As noted above, the critical issue of computational efficiency is addressed by the Symmetric-Galerkin approximation. This method relies on hypersingular equations to produce a symmetric coefficient matrix. The symmetry can be exploited, in both matrix construction and solution, to provide the efficiency needed to counterbalance the high computational cost of the extra boundary integration [13, 53]. Roughly speaking, Symmetric-Galerkin is competitive with collocation, and will be faster for sufficiently large scale problems. For two dimensional problems, the crossover point where Symmetric-Galerkin becomes more efficient is known to occur at reasonable sized problems, around $200-300$ elements [13, 53]. The main objection to use of Galerkin in applications is therefore removed, and it is now an attractive alternative to collocation. Moreover, it can be argued that for some applications, most notably fracture analysis [22], it is the method of choice.

Two additional benefits provided by the Galerkin approach, namely tangential derivative evaluation and improved corner treatment, will be highlighted in this chapter. Applications will sometimes require a 'post-processing' evaluation of boundary derivatives, *e.g.*, the tangential component of the electric field or the complete stress tensor on the boundary. Direct evaluation with collocation once again is faced with the $C^1$ condition and indirect methods [54] are inefficient. A Galerkin formulation has been shown to be quite successful [55]. Second, as might be expected, collocating hypersingular integrals at a corner is not an easy matter. The corner interpolation constraints analogous to the smooth surface $C^1$ condition [56, 57] are complicated, and even more difficult to implement than differentiability. As a consequence, treating corners involving only Dirichlet boundary conditions is a major problem [58], as is the evaluation of (the multiple) tangential derivatives at a corner. Moreover, depending upon the supplied boundary data, collocation approximations are known to produce inaccurate solutions in the vicinity of a corner [59]. Galerkin bypasses these difficulties, the treatment of corners is relatively straightforward and simple, and our experience has been that accurate corner solutions are obtained. Some of the numerical results presented below will address these two important aspects of boundary integral analysis.

Not surprisingly, the prevalence of the collocation approach in applications has meant that most of the singular integration literature has focused on this technique [34]. However, over the past several years, the evaluation of Galerkin singular integrals has received some attention, and a variety of approaches have been employed. A principal technique has been *regularization*, also commonly used for collocation integrals [60]. By reformulating the integral either by integrating by parts [61, 62, 63] or by using simple solutions [64], the kernels are at worst weakly singular and can be dealt with numerically. More direct methods

include entirely numerical [65], analytical for linear elements [66], and combined analytic/numeric for linear [67] or curved elements [13].

This chapter presents a direct scheme for evaluating Galerkin singular integrals that relies primarily on analytic integration. This is a somewhat different method, and hopefully a simpler presentation, than that in [13]. Although all of the singular integration techniques cited above are valid, and the choice of a method is to some degree a matter of taste, the direct approach has some beneficial features. The direct method is quite general, immediately applicable to any Green's function, and to either linear or curved interpolations. Second, the analytic integration allows exact cancellation of the potentially divergent terms which arise, and thus the method is reliable. This also helps with efficiency: the integrals that are computed numerically are completely non-singular, and thus *low order* Gauss quadrature can be safely invoked. Moreover, symbolic computation allows a very simple derivation of the analytic integration formulas, even for complicated kernels [68]. Finally, and perhaps the most important aspect, is that these techniques extend, more or less directly, to three-dimensions. The present contribution will consider only two dimensional problems, the three dimensional analysis will be presented elsewhere [69].

An attempt is made to keep this article as self-contained as possible. The next section defines the Symmetric-Galerkin approximation, and Section 3 establishes the necessity of the $C^1$ condition for collocation. The core of this chapter is Section 4, which describes, in the context of the Laplace equation, the singular integration procedures for a linear element. The subsequent section treats the more complicated Green's function for orthotropic elasticity, and results for several fracture calculations are presented. The extension of the integration methods to higher order curved elements is provided in Section 6, while Section 7 discusses the evaluation of tangential derivatives. In Section 8, these methods are applied to study an important problem in micro-electronics, void evolution in aluminum thin film interconnects. Finally, it will come as no surprise that some concluding remarks are to be found in the Conclusions.

## 2 Symmetric-Galerkin

To define notation, and for completeness, this section will describe the Symmetric-Galerkin approximation for the two-dimensional Laplace equation, $\nabla^2\phi = 0$. The extension to other equations is immediate. The boundary integral equations for potential $\phi$ and normal flux $\partial\phi/\partial\mathbf{n} = \nabla\phi\bullet\mathbf{n}$ are

$$\mathcal{P}(P) \equiv \phi(P) + \int_\Gamma \phi(Q)\frac{\partial G}{\partial \mathbf{n}}(P,Q)\,dQ - \int_\Gamma G(P,Q)\frac{\partial \phi}{\partial \mathbf{n}}\,dQ = 0 \ , \qquad (1)$$

and

$$\mathcal{F}(P) \equiv \frac{\partial \phi(P)}{\partial \mathbf{N}} + \int_\Gamma \phi(Q)\frac{\partial^2 G}{\partial \mathbf{N}\partial \mathbf{n}}(P,Q)\,dQ - \int_\Gamma \frac{\partial G}{\partial \mathbf{N}}(P,Q)\frac{\partial \phi}{\partial \mathbf{n}}(Q)\,dQ = 0 \ . \quad (2)$$

Here $\mathbf{n} = \mathbf{n}(Q)$, $\mathbf{N} = \mathbf{N}(P)$ denote the unit outward normal on the boundary curve $\Gamma$ of the domain $\mathcal{D}$, $P$ and $Q$ points on $\Gamma$. It is customarily stated that these equations are valid for $P \in \mathcal{D}$, and that for $P$ on the boundary there is a 'boundary

angle' (solid angle in three dimensions) or a 'free term' coefficient multiplying the leading terms $\phi(P)$ and $\partial\phi/\partial\mathbf{n}(P)$, respectively. However, conceptually, and computationally, it seems easier to adopt the view that these equations are valid for $P \in \mathcal{D}$, and that for $P \in \Gamma$, one examines the limiting value of the integrals as $P$ approaches the boundary. This is especially sensible for the hypersingular equation, Eq. (2), as this expression was obtained by interchanging the derivative and the integral, clearly illegal for $P \in \Gamma$. Thus, writing this equation for $P$ on the boundary is a mistake that regularization, or some other procedure, must then struggle to undo. It seems preferable not to make this error in the first place. Moreover, the limit to the boundary interpretation works equally well for Eq. (1), and it provides some computational advantages – the 'free term' coefficients, which are sometimes troublesome to compute [70], are handled automatically [71]. Finally, the limit process has also proved useful in the analysis of crack tip expansions [72].

The fundamental solution $G(P,Q)$ is usually taken as the point source potential

$$G(P,Q) = -\frac{1}{2\pi}\log\|Q-P\| \ , \tag{3}$$

and for Symmetric-Galerkin it is important to note the symmetry properties

$$\begin{aligned} G(P,Q) &= G(Q,P) \\ \frac{\partial G}{\partial \mathbf{n}}(P,Q) &= -\frac{\partial G}{\partial \mathbf{N}}(P,Q) = \frac{\partial G}{\partial \mathbf{N}}(Q,P) \\ \frac{\partial^2 G}{\partial \mathbf{n}\partial \mathbf{N}}(P,Q) &= \frac{\partial^2 G}{\partial \mathbf{n}\partial \mathbf{N}}(Q,P) \end{aligned} \tag{4}$$

Collocation reduces Eq. (1) and Eq. (2) to a finite linear system by enforcing these equations at the nodal points $\{P_j\}$ which define the discretized geometry,

$$\begin{aligned} \mathcal{P}(P_k) &= 0 \, , \\ \mathcal{F}(P_l) &= 0 \, . \end{aligned} \tag{5}$$

In a weighted residual formulation, however, the integral equations are only enforced 'on average', in the form

$$\int_\Gamma \psi_k(P)\mathcal{P}(P)\,dP = 0 \ , \tag{6}$$

$$\int_\Gamma \psi_l(P)\mathcal{F}(P)\,dP = 0 \ , \tag{7}$$

where $\psi_j(P)$ are selected weight functions. In a Galerkin scheme, these weights are the shape functions employed in interpolating the boundary functions $\phi$ and its normal derivative $\partial\phi/\partial\mathbf{n}$. For a simple linear element, these functions are illustrated in Fig. 1.

Symmetry of the coefficient matrix for a general mixed boundary value problem is achieved by the following simple prescription. The potential equation is employed on the Dirichlet surface $\Gamma^d$, and the negative of the flux equation is used on the Neumann surface $\Gamma^n$, $\Gamma = \Gamma^d + \Gamma^n$. In block matrix form this can be

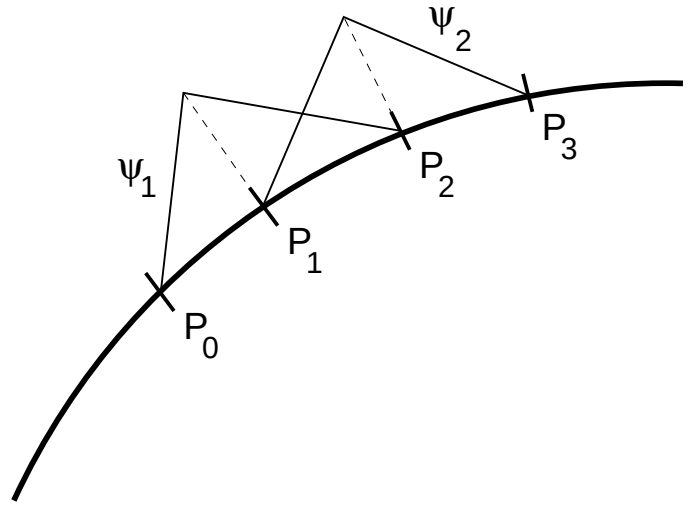


Figure 1: Illustration of Galerkin weight functions for a linear approximation.

written as

$$\begin{pmatrix} h^{dd} & h^{dn} \\ -h^{nd} & -h^{nn} \end{pmatrix} \begin{pmatrix} \phi^d \\ \phi^n \end{pmatrix} - \begin{pmatrix} g^{dd} & g^{dn} \\ -g^{nd} & -g^{nn} \end{pmatrix} \begin{pmatrix} \frac{\partial \phi}{\partial \mathbf{n}}^d \\ \frac{\partial \phi}{\partial \mathbf{n}}^n \end{pmatrix} = 0 \ . \tag{8}$$

The first row represents the Eq. (6) written on $\Gamma^d$ surface, the second from Eq. (7) on $\Gamma^n$. The columns have similar meaning, the first column arising from the $Q$ integration over $\Gamma^d$. As the unknowns are flux on $\Gamma^d$ and potential on $\Gamma^n$, the coefficient matrix becomes

$$\begin{pmatrix} -g^{dd} & h^{dn} \\ g^{nd} & -h^{nn} \end{pmatrix} \ , \tag{9}$$

and the symmetry of this matrix follows from Eq. (4). As noted above, the symmetry is crucial, as it can be exploited to offset the computational burden of the double boundary integration.

As a final comment, note that the Symmetric-Galerkin prescription does not immediately apply to the important class of problems where the domain consists of sub-domains having different physical properties, *e.g.*, elastic constants. In this case, the interfaces between the homogeneous sub-domains have no prescribed data, and both physical variables must be computed. Fortunately, the Symmetric-Galerkin method does extend in a natural way to cover interface problems [73].

## 3 $C^1$ Condition

The $C^1$ condition associated with the treatment of hypersingular equations is the main weakness of collocation, and hence a principal argument in favor of Galerkin. We therefore digress somewhat to present a simple demonstration of the necessity of this condition. The additional justification for subjecting the

reader to this exercise is that it illustrates the *limit to the boundary* and analytic integration procedures that will be used in Section 4 to define and evaluate the singular integrals. To establish the $C^1$ condition, evaluation of the hypersingular integral will be attempted for $P$ a point on a flat boundary segment. It will be seen that, without differentiability, the integral fails to exist. This is essentially the two dimensional version of the calculation presented in [26].

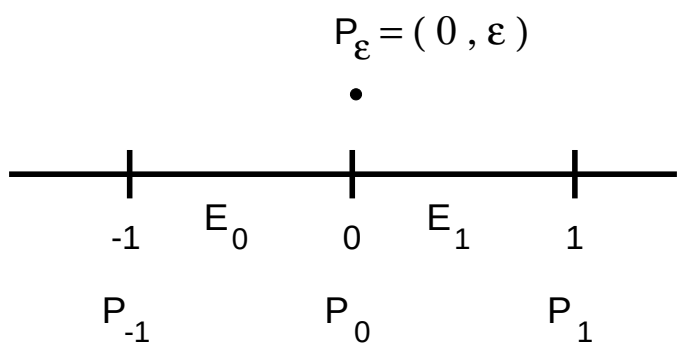


Figure 2: Limit to the boundary for collocating the hypersingular integral.

Consider, as shown in Fig. 2, a flat boundary segment lying along the $x-$axis, consisting of the interval $[-1, 1]$. This segment is divided into the two elements $E_0 = [-1, 0]$ and $E_1 = [0, 1]$, outward normals $\mathbf{n} = \mathbf{N} = (0, -1)$, with nodes $P_{-1} = (-1,\ 0)$, $P_0 = (0,\ 0)$, and $P_1 = (1,\ 0)$. Note that for $P = P_0$, the hypersingular integral

$$-\frac{1}{2\pi}\int_{E_0+E_1} \phi(Q)\left\{-\frac{\mathbf{N}\bullet\mathbf{n}}{r^2} + 2\frac{(\mathbf{n}\bullet R)(\mathbf{N}\bullet R)}{r^4}\right\} dQ \ . \tag{10}$$

simply does not exist. The limit to the boundary is effected by replacing $P_0$ with the interior point

$$P_\varepsilon = P_0 - \varepsilon\mathbf{N} \ . \tag{11}$$

With $P$ off the boundary the integral exists, and then the limit $\varepsilon \to 0$ can be considered. Thus, in this case $R = Q - P_\varepsilon = Q - (0, \varepsilon)$.

On $E_0$ the linear interpolation for $\phi$ is $\phi(Q) = \phi(Q(t)) = \phi_0 + t(\phi_0 - \phi_{-1})$, where $\phi_j = \phi(P_j)$ and $t \in [-1,\ 0]$. For $E_1$, $\phi(Q) = \phi_0 + t(\phi_1 - \phi_0)$, $t \in [0,\ 1]$. It is only the linear terms (multiplying $t$) that are of interest here, and the required integrals over $E_0$ and $E_1$ are

$$\begin{aligned}
\mathcal{I}_0 &= -\frac{\phi_0 - \phi_{-1}}{2\pi}\int_{-1}^{0} t\left\{-\frac{1}{t^2+\varepsilon^2} + 2\frac{2\varepsilon^2}{(t^2+\varepsilon^2)^2}\right\} dt \ , \\
\mathcal{I}_1 &= -\frac{\phi_1 - \phi_0}{2\pi}\int_{0}^{1} t\left\{-\frac{1}{t^2+\varepsilon^2} + 2\frac{2\varepsilon^2}{(t^2+\varepsilon^2)^2}\right\} dt \ .
\end{aligned} \tag{12}$$

Simple calculus results in

$$\begin{aligned}
\mathcal{I}_0 &= \quad (\phi_0 - \phi_{-1})\log(\varepsilon) + \cdots \ , \\
\mathcal{I}_1 &= -(\phi_1 - \phi_0)\log(\varepsilon) + \cdots \ .
\end{aligned} \tag{13}$$

Our only concern is the potentially divergent terms, and thus the contributions which are well behaved as $\varepsilon \to 0$ are suppressed. For the hypersingular integral to have a finite value, the two $\log(\varepsilon)$ terms must cancel, and thus it follows that

$$\phi_0 - \phi_{-1} = \phi_1 - \phi_0 \ . \tag{14}$$

The expressions on the left and right are in fact the tangential derivatives of $\phi(Q)$ on $E_0$ and $E_1$, respectively, and thus for a non-$C^1$ interpolation at $P_0$ the hypersingular integral does not exist.

More precisely, without a differentiable interpolation of $\phi$ at $P_0$, there is no way to define the integral in Eq. (10) so that it is *continuous from the interior*. The Hadamard Finite Part [15, 74, 75, 76] will assign a value to this integral, essentially by ignoring the $\log(\varepsilon)$ singularity, but lacking continuity to the boundary, the physical relevance of this definition is dubious. More important, perhaps, is that hypersingular boundary integral calculations employing a $C^0$ element can give nonsensical solutions.

For Galerkin, the additional boundary integration reduces the strength of the singularity, and thus the hypersingular kernel should only require a $C^0$ interpolation. This will be verified in the next section, again by simply evaluating the integrals directly.

## 4 Singular Integrals: Linear Element

A Galerkin calculation requires the evaluation of integrals for each pair of elements $\{E_P,\ E_Q\}$ and, as illustrated in Fig. 3, two types of singular integrals arise in a two dimensional calculation. The case $E_P = E_Q$ is designated *coincident*, and *adjacent* refers to $E_P \neq E_Q$ but sharing a common node. In three dimensions, there are two varieties of adjacent integration, adjacent elements can share a common edge or a common vertex. In this section, the integration procedures are first presented in detail for the Laplace equation. The next section will discuss, in somewhat less detail, the analysis for orthotropic elasticity.

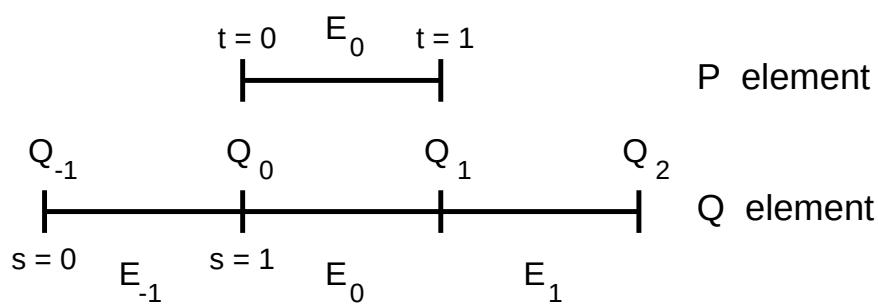


Figure 3: For $E_P = E_0$, the coincident singular integration is $E_Q = E_0$, and the adjacent singular integrations are $E_Q = E_1$ and $E_Q = E_{-1}$.

A goal of this chapter is to demonstrate that Galerkin singular integral evaluation, often perceived as a far more complicated undertaking than for collocation, is a reasonably straightforward process. Unfortunately, to make this case,

a discussion of the details of the singular integration process cannot be avoided. We have opted to present this material by displaying the Maple scripts used to construct the boundary integral programs. As the Maple operations are usually named sensibly, it is hoped that these scripts are mostly self-explanatory. Comments will be provided as needed. In an attempt to make reading through this material less boring, we have, in some cases, omitted parts of the scripts that are primarily cosmetic in nature, aimed at simplifying the appearance of the formulas.

It will become clear that symbolic computation is not absolutely necessary to carry out the analysis of the Laplace singular integrals. With integration tables, and a moderate amount of pain and suffering, it is certainly possible to develop the formulas by hand. However, for more complicated kernels, symbolic computation is virtually essential. Moreover, even for the simple Laplace case, the time and effort required to construct and debug a boundary integral code is most likely considerably less if symbolic computation is employed.

As indicated in Fig. 3, the parameters for the $P$ and $Q$ integrations will be denoted by $t \in [0,1]$ and $s \in [0,1]$, respectively. The linear element approximation is defined by the boundary and surface function approximations, which for the element $E_0 = \{Q_0, Q_1\}$ are given by

$$\begin{aligned} Q(s) &= (1-s)Q_0 + sQ_1 = M_1(s)Q_0 + M_2(s)Q_1 \\ \phi(Q(s)) &= M_1(s)\phi(Q_0) + M_2(s)\phi(Q_1) \\ \frac{\partial \phi}{\partial \mathbf{n}}(Q(s)) &= M_1(s)\frac{\partial \phi}{\partial \mathbf{n}}(Q_0) + M_2(s)\frac{\partial \phi}{\partial \mathbf{n}}(Q_1) \ . \end{aligned} \tag{15}$$

As shown in Fig. 1, the Galerkin weighting functions $\psi_k(P)$ are also defined by the linear shape functions, $M_1(z) = 1-z$, $M_2(z) = z$. Thus, at the node $P_1 = Q_1$,

$$\psi_{P_1}(t) = \begin{cases} t & P \in E_0 \\ 1-t & P \in E_1 \\ 0 & \text{otherwise} \end{cases} \ . \tag{16}$$

The general form of the double integrals to be computed can be expressed as

$$\int_0^1 M_k(t) J_p(t) \int_0^1 M_j(s) J_q(s) \mathcal{H}(s,t)\, ds\, dt \ , \tag{17}$$

where $\mathcal{H}$ can be the Green's function or one of its derivatives and $1 \le k \le 2$, $1 \le j \le 2$. Note that one major simplification of the linear element is that the jacobians $J_p$ and $J_q$ are constants.

## 4.1 Coincident Integration

Although the coincident integration has a line of singularities along $t = s$, this is actually a somewhat simpler situation than the adjacent integration with its single singular point. We therefore begin the trek through the singular integral evaluations with this easier task. All kernel functions contain the distance $r = \|R\| = \|Q - P\|$, and for the element $E_P = E_Q$ defined by the nodes $Q_0 = (x_0, y_0)$ and $Q_1 = (x_1, y_1)$, Eq. (15) yields

$$r(s,t) = \|Q(s) - P(t)\| = a|s-t| \tag{18}$$

where $a = J_q = J_p = \left((x_1 - x_0)^2 + (y_1 - y_0)^2\right)^{1/2}$.

### 4.1.1 G

Substituting Eq. (18) and Eq. (3) into Eq. (6), the integrals to be evaluated are

$$-\frac{a^2}{2\pi}\int_0^1 M_k(t)\int_0^1 M_j(s)\log\left(a|s-t|\right)\,ds\,dt\ , \tag{19}$$

and the final result is

$$\begin{aligned} -\frac{a^2}{8\pi}\left[-\frac{7}{4}+\log(a)\right]\ , \qquad & k = j \\ -\frac{a^2}{8\pi}\left[-\frac{5}{4}+\log(a)\right]\ , \qquad & k \neq j\ . \end{aligned} \tag{20}$$

The simple, and mostly self-explanatory, Maple script that was used to obtain this result is:

```
ker1 := ln(a*(t-s));
ker2 := ln(a*(s-t));
b1   := int((1-s)*ker1,s=0..t) + int((1-s)*ker2,s=t..1);
b2   := int(s*ker1,s=0..t) + int(s*ker2,s=t..1);
b11  := int((1-t)*b1,t=0..1);
b12  := int(t*b1,t=0..1);
b21  := int((1-t)*b2,t=0..1);
b22  := int(t*b2,t=0..1);
```

As might be guessed, `ln` is the logarithm and `int` is the integration operator. The splitting of the inner $s$ integration into two pieces is to help Maple around the absolute value that appears inside the logarithm.

### 4.1.2 First derivative of G

Differentiating the Green's function with respect to $Q$, the potential integral in Eq. (6) becomes

$$-\frac{a}{2\pi}\int_0^1 M_k(t)\int_0^1 M_j(s)\frac{J_q\mathbf{n}\bullet R}{r^2}\,ds\,dt\ . \tag{21}$$

The factor $a$ in front is $J_p$. It is convenient in this case to attach $J_q$ to the kernel function, as $J_q\mathbf{n}$ is simpler to compute than the unit normal. For the linear element coincident integration it would seem that this is a trivial calculation: the vector $R = Q - P$ is the unnormalized tangent vector and therefore orthogonal to the normal $\mathbf{n}$. Hence, Eq. (21) is identically zero. This, however, neglects the fact that for $P \in \Gamma$, Eqs. (1) and (6) were valid provided the singular integrals were defined as a limit to the boundary. The singularity in $G$ is weak enough that the integral exists for $P$ on the boundary, and consequently a limit process was not necessary.

In the boundary limit process, the point $P$ is first replaced by the interior point $P - \varepsilon\mathbf{n}$ (recall that $\mathbf{n}$ is an outward normal). The integrals, which are now

nonsingular, can be evaluated and the limit $\varepsilon \to 0$ considered. The implementation of this process is easily explained by annotating the Maple script. The first section of code sets up the kernel function, the variable `eps` playing the role of $\varepsilon$, and then computes the $Q$ integration:

```
p1  := (1-t)*x0 + t*x1 - eps*(y1-y0);
p2  := (1-t)*y0 + t*y1 - eps*(x0-x1);
q1  := (1-s)*x0 + s*x1;
q2  := (1-s)*y0 + s*y1;
r1  := q1 - p1;
r2  := q2 - p2;
rsq := r1*r1 + r2*r2;
rsq := collect(rsq,[s,t]);
jnr := (y1-y0)*r1 + (x0-x1)*r2;
ker := jnr/rsq;
c1  := int((1-s)*ker,s=0..1);
```

Note that, for brevity, we only consider the shape function $M_1(s)$, as $M_2(s)$ follows in the same manner. At this point the limit can be evaluated, and this requires informing Maple, via the substitution operator `subs`, that $\lim \tan(\pm 1/\varepsilon) = \pm\pi/2$ and that $\varepsilon > 0$:

```
c1  := subs(arctan(t/sqrt(eps^2))=pi/2,c1);
c1  := subs(arctan((-1+t)/sqrt(eps^2))=-pi/2,c1);
c1  := subs(1/sqrt(eps^2)=1/eps,c1);
c1  := expand(c1);
c1  := subs(sqrt(eps^2)=eps,c1);
c1  := subs(eps=0,c1);
```

Finally, the $P$ integration can be carried out:

```
b11 := int(expand((1-t)*c1),t=0..1);
b21 := int(expand(t*c1),t=0..1);
```

The result for Eq. (21) is simply

$$\begin{array}{lll} -\dfrac{a}{6}\,, & k & = & j \\ -\dfrac{a}{12}\,, & k & \neq & j\,. \end{array} \tag{22}$$

The singular integral has been evaluated directly, without the complicated and mysterious 'symmetric bumping out the surface' Cauchy Principal Value procedure that is commonly used [4]. The 'angle coefficient' that results from CPV (usually included explicitly in the boundary integral statement) can sometimes be troublesome to compute [70]. Here it is automatically taken care of by the direct calculation. The advantages of this limit approach, for collocation or Galerkin, are further discussed in [71]. Finally, note that the single derivative kernel in the hypersingular flux equation Eq. (7) is $\partial G/\partial \mathbf{N}$, and as $\mathbf{n} = \mathbf{N}$ for coincident elements, there is no need to discuss this integral.

### 4.1.3 Second derivative of G

The $\partial G/\partial \mathbf{n}$ integral, which is somewhat contentious for collocation, is well behaved for Galerkin, and thus nothing very interesting has emerged as yet from the analytic integrations. However, the Galerkin integration of the hypersingular kernel,

$$-\frac{1}{2\pi}\int_0^1 M_k(t)\int_0^1 M_j(s)\left\{-\frac{(J_p\mathbf{N})\bullet(J_q\mathbf{n})}{r^2}+2\frac{(J_q\mathbf{n}\bullet R)(J_p\mathbf{N}\bullet R)}{r^4}\right\}ds\,dt\ , \quad (23)$$

will resemble, in the strength of the singularity, the collocation CPV integral. This term then should not prove boring. The initial Maple coding for setting up the geometry and the $\varepsilon$ limit is the same as the first section of coding above, and will not be repeated. For $k = j = 1$, the $Q$ integration and limit $\varepsilon \to 0$ can proceed as before:

```
jn1 := y1 - y0;
jn2 := x0 - x1;
ker := -(jn1*jn1 + jn2*jn2)/rsq + 2*(jn1*r1+jn2*r2)^2/(rsq*rsq);
b11  := int((1-t)*(1-s)*ker,s=0..1);
b11  := expand(b11);
b11  := subs(sqrt(eps^2)=eps, b11);
b11  := subs(1/sqrt(eps^2)=1/eps, b11);
b11  := subs(arctan(t/eps)=pi/2,b11);
b11  := subs(arctan((t-1)/eps)=-pi/2,b11);
b11  := subs(eps=0,b11);
b11  := subs(ln(t^2-2*t+1)=2*ln(1-t),b11);
```

At this point however, the $P$ integration will fail because of the presence of a $t^{-1}$ term (finally, something interesting!). This is not surprising, as this is the divergent term that CPV gets rid of for collocation. This divergent $t^{-1}$ contribution will eventually cancel: in terms of the notation in Fig. 3, if the coincident integration is $E_P = E_Q = E_0$, it will be seen that the balancing term appears in the *left adjacent integration* $E_P = E_0$, $E_Q = E_{-1}$. This term is therefore explicitly removed, and the analytic integration proceeds as

```
b11  := b11 - 1/t;
b11  := int(b11,t=0..1);
```

It is easy to see that $t^{-1}$ arises from the constant term in the product of the shape functions, and therefore multiplies $\phi(Q_0)$. By contrast, in Section 3, the $\log(\varepsilon)$ divergence occurred in the linear term. Thus Galerkin only requires continuity between elements to achieve cancellation and finite integrals. Similarly, the $k = j = 2$ term in Eq. (23) will produce a $(1-t)^{-1}$ contribution, multiplying $\phi(Q_1)$, which will disappear once the *right adjacent integration* is computed. For $k \neq j$, the product of the two shape functions is zero at both endpoints, and thus no divergent terms arise. The final result for Eq. (23) is

$$\begin{array}{lll} \dfrac{1}{4\pi}\,, & k & = & j \\ -\dfrac{1}{4\pi}\,, & k & \neq & j\ . \end{array} \quad (24)$$

A significant advantage of the direct limit approach is that the canceling divergent terms can be identified and removed from the calculation. The cancellation is therefore achieved *exactly*, and each individual integral is a well defined quantity. The alternative, approximate quadrature of divergent integrals and effecting the cancellation numerically, is not an attractive proposition.

### 4.2 Adjacent Integration

Thus far the integrations have been relatively trivial, and complete analytical evaluation of the double integral was possible. Moreover, the resulting exact formulas are simple enough that computation time is not an issue, and thus analytic integration is the obvious choice. For the adjacent singular integration, the singularities are necessarily weaker, being at a single point in the two-dimensional $\{t, s\}$ parameter space, but the integrands are less simple. As a consequence, we adopt a hybrid method, the analytical work restricted to one dimension in parameter space, and one dimension left to numerical means.

It is convenient to introduce a polar coordinate transformation, $\{t,\ s\} \rightarrow \{\rho,\ \theta\}$ centered at the singular point. The nasty part of the function is associated with $\rho$, and the $\rho\ d\rho\ d\theta$ jacobian helps to reduce the strength of the singularity. The $\rho$ integration will be performed analytically, leaving a smooth function of $\theta$ for the numerical quadrature.

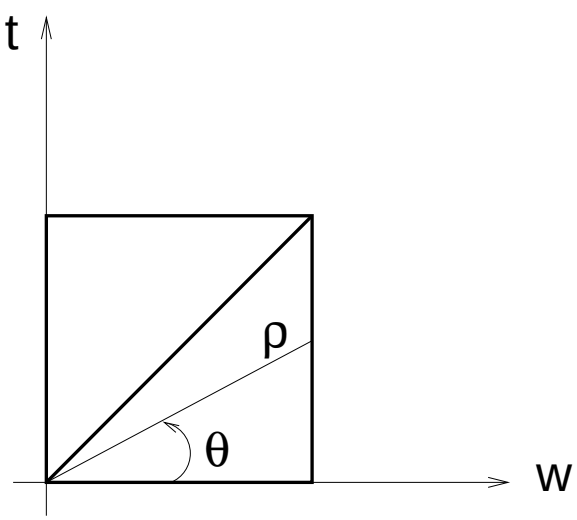


Figure 4: Polar coordinates for the adjacent singular integrations.

We treat only the *left adjacent* case, $E_P = E_0$, $E_Q = E_{-1}$, the right adjacent can be treated analogously. Or, even more simply, reverse direction of the elements $E_P = E_0$ and $E_Q = E_1$ and use the left adjacent algorithm, making a needed sign change to account for the wrong orientation. Referring again to Fig. 3, the singularity is at $t = 0$, $s = 1$. Changing variables, $w = 1 - s$, the singular point is at the origin $t = w = 0$, and polar coordinates is then defined

by $w = \rho\cos(\theta)$, $s = \rho\sin(\theta)$. As indicated in Fig. 4,

$$\int_0^1 \int_0^1 \cdots ds\ dt \rightarrow \int_0^{\frac{\pi}{4}} \int_0^{\sec(\theta)} \cdots\ \rho\ d\rho\ d\theta + \int_{\frac{\pi}{4}}^{\frac{\pi}{2}} \int_0^{\csc(\theta)} \cdots\ \rho\ d\rho\ d\theta\ . \qquad (25)$$

In the following Maple script, appearing in all adjacent integrations, `xm1` stands for $x_{-1}$, the $x$-coordinate of $Q_{-1}$, and the distance function becomes $r^2 = a^2\rho^2$, where $a$ is a function of $\theta$.

```
q1 := w*xm1 + (1-w)*x0;
q2 := w*ym1 + (1-w)*y0;
p1 := (1-t)*x0 + t*x1;
p2 := (1-t)*y0 + t*y1;
r1 := q1 - p1;
r2 := q2 - p2;
rsq := r1*r1 + r2*r2;
rsq := subs(w=rho*ct,t=rho*st,rsq);
asq := expand(rsq/rho^2);
```

### 4.2.1 G and its first derivative

As the integration of these two terms is straightforward, we discuss them together. For $G(P,Q)$, the additional coding is

```
ker  := rho*ln(a*rho);
b11  := int((1-rho*st)*rho*ct*ker,rho=0..L):
b12  := int((1-rho*st)*(1-rho*ct)*ker,rho=0..L):
b21  := int(rho*st*rho*ct*ker,rho=0..L):
b22  := int(rho*st*(1-rho*ct)*ker,rho=0..L):
```

Here, $L$ stands for the upper limit $\sec(\theta)$ or $\csc(\theta)$, depending upon the value of $\theta$. For the normal derivative of $G(P,Q)$, including the $\rho$ factor from the jacobian with the kernel makes this term independent of $\rho$. The $\rho$ integration therefore simply reduces to the product of the shape functions, and as this is a trivial task, this calculation is omitted. The $\partial G/\partial \mathbf{N}$ integral from the flux equation follows exactly as above and is likewise omitted.

### 4.2.2 Second derivative of G

With the exception of $k = 1$, $j = 2$, the product of the shape functions is zero at the singular point $Q_0$, and as a consequence these integrals in Eq. (23) are perfectly well behaved. These contributions, and the non-constant terms from $k = 1$, $j = 2$, namely $M_1(t)M_2(s) - 1$, can be handled as above. We therefore focus solely on the constant term integration arising from $k = 1$, $j = 2$. As a balancing divergent $-t^{-1}$ term is expected, polar coordinates is not an option, and we return to integrating over $\{t,\ s\}$. The compensation is that a complete analytic integration of this term is possible.

Of all the calculations, this is the most complicated, and the Maple coding will require some explanation.

```
q1     := w*xm1 + (1-w)*x0;
q2     := w*ym1 + (1-w)*y0;
p1     := (1-t)*x0 + t*x1;
p2     := (1-t)*y0 + t*y1;
r1     := q1 - p1;
r2     := q2 - p2;
rsq    := r1*r1 + r2*r2;
rsq    := collect(rsq,w);
a0     := coeff(rsq,w,0);
a1     := coeff(rsq,w,1);
a2     := coeff(rsq,w,2);
betasq := expand((4*a2*a0-a1^2)/t^2);
rsq    := c2*w*w + c1*w +c0;
ker    := -(jnjN)/rsq + 2*(jnq1*r1+jnq2*r2)*
                (jnp1*r1+jnp2*r2)/(rsq*rsq);
b12s   := int(ker,w=0..1);
```

Note that $r^2 = a_2 w^2 + a_1 w + a_0$; these polynomial coefficients are replace by new constants $\{c_j\}$ merely to simplify the appearance of the formulas. The integration results in two types of rational function terms, one with denominators which are not zero at $t = 0$, and one with terms of the form $t^k$. It is these latter terms that we are most interested in, and thus a change of variables, $t^{-k} \to v^{-k}$ is made so that these contributions can be isolated.

```
b12s   := subs(arctan(c1/sqrt(4*c2*c0-c1^2))=at1,b12s):
b12s   := subs(arctan((c1+2*c2)/sqrt(4*c2*c0-c1^2))=at2,b12s):
b12s   := subs((4*c2*c0-c1^2)^(-5/2)=beta^(-5)*t^(-5),b12s):
b12s   := subs((4*c2*c0-c1^2)^(3/2)=beta^(3)*t^(3),b12s):
b12s   := subs(c0=a0,c1=a1,c2=a2,b12s):
b12s   := subs(t^6=v^6,t^5=v^5,t^4=v^4,t^(-5)=v^(-5),b12s):
b12s   := subs(jnjN=(y0-ym1)*(y1-y0)+(xm1-x0)*(x0-x1),b12s):
b12s   := expand(b12s):
b12s   := collect(b12s,v):
cf1    := coeff(b12s,v,-1);
cf1    := normal(subs(1/beta^2=1/betasq,cf1));
b12s   := b12s - cf1/v;
```

As expected, the coefficient of the $1/t$ term, `cf1`, is equal to $-1$, and cancels with the coincident integration. After integrating `b12s` with respect to $t$, the final result is

$$-\frac{1}{4\pi}\log\left(\frac{(x_1 - x_{-1})^2 + (y_1 - y_{-1})^2}{J_q^2}\right) \quad . \tag{26}$$

The process of reducing the answer to this simple form is not straightforward, but not especially interesting. We therefore omit the details.

### 4.3 Accuracy

Simple test calculations have been carried out to verify the correctness of the above procedures. Consider first a Dirichlet problem on the unit disk, with

boundary values $\phi = x^2 - y^2$. Table 1 compares the maximum and $L^2$ errors in the computed normal flux for Symmetric-Galerkin and collocation approximations, both employing a linear element approximation. The $L^2$ error is defined as

$$\left( \frac{1}{M} \sum_{k=1}^{M} e_k^2 \right)^{1/2} , \tag{27}$$

where $M$ is the number of nodes and $e_k$ is the error at node $k$. Results for four uniform discretizations of the circle are reported, $M = 30,\ 60,\ 150,\ 300$. In both methods, all numerical quadratures were computed using a 4-point Gauss rule, and the singular integrals in the collocation method were calculated analytically. In this case, the Symmetric-Galerkin results are significantly more accurate than collocation.

| M | Symmetric-Galerkin | | Collocation | |
|---|---|---|---|---|
| | Max | $L^2$ | Max | $L^2$ |
| 30 | .00326354 | .00230768 | .01518792 | .01073948 |
| 60 | .00086900 | .00061446 | .00417751 | .00295394 |
| 150 | .00014453 | .00010220 | .00070568 | .00049900 |
| 300 | .00003703 | .00002619 | .00017957 | .00012698 |

Table 1: A comparison of Symmetric-Galerkin and collocation nodal errors for a Dirichlet problem on the unit disk.

For the Dirichlet boundary conditions, the Symmetric-Galerkin method employs the potential equation. To examine the performance of the hypersingular flux equation, a Neumann problem is solved exterior to the unit disk. The chosen exact solution is $\phi = x/(x^2 + y^2)$, which also turns out to be the form of the normal flux boundary condition. The errors in the computed potential are shown in Table 2, and once again Symmetric-Galerkin is more accurate than collocation. Note that the collocation solution was obtained using the potential equation – the hypersingular equation cannot be used with the $C^0$ linear element approximation.

| M | Symmetric-Galerkin | | Collocation | |
|---|---|---|---|---|
| | Max | $L^2$ | Max | $L^2$ |
| 30 | .00191174 | .00135180 | .00941169 | .00665506 |
| 60 | .00047500 | .00033588 | .00231805 | .00163911 |
| 150 | .00009619 | .00006802 | .00036755 | .00025990 |
| 300 | .00006431 | .00004547 | .00009158 | .00006476 |

Table 2: A comparison of Symmetric-Galerkin and collocation nodal errors for a Neumann problem on the domain exterior to the unit disk.

That Galerkin is more accurate than collocation is not surprising. Similar behavior was observed for two dimensional elasticity (using a non-symmetric Galerkin formulation) by de Paula and Telles [67].

# 5 Orthotropic Elasticity

As discussed in the introduction, hypersingular equations were developed primarily in response to the need for an efficient boundary integral fracture analysis algorithm. Crack calculations are therefore a main motivation for developing the Galerkin method. To present some computational fracture results, this section will present a *brief* discussion of the boundary integral equations for orthotropic elasticity. Further details can be found in [22, 77, 78].

The singularities arising in the elastic analysis are no different from those in the corresponding point source potential and its derivatives, and thus there is no substantive change in the nature of the singular integrations. However, the fundamental displacement solution $U(P,Q)$ involves two logarithmic terms rather than the one in $G(P,Q)$, and moreover is a tensor of order 2. The expressions for the derivative kernels are therefore more numerous and rather longer than for the Laplace equation. Thus, symbolic computation is, if not absolutely essential, at least highly useful for simplifying the construction of the algorithm.

## 5.1 Orthotropic Boundary Integral Equations

The boundary integral formulation for two dimensional orthotropic elasticity was developed by Rizzo and Shippy [78], and we follow their presentation. If $u_j$ and $\sigma_{jk}$ denote the components of the displacement vector and stress tensor, the plane stress constitutive relationship is given by

$$\begin{aligned} \sigma_{11} &= c_{11}u_{1,1} + c_{12}u_{2,2} \\ \sigma_{22} &= c_{12}u_{1,1} + c_{22}u_{2,2} \\ \sigma_{12} &= c_{66}(u_{1,2} + u_{2,1}) \ , \end{aligned} \tag{28}$$

where $c_{ij}$ are material constants. The Navier–Cauchy equilibrium equations, in the absence of body forces, are

$$\begin{aligned} c_{11}u_{1,11} + (c_{12} + c_{66})u_{2,12} + c_{66}u_{1,22} &= 0 \\ c_{22}u_{2,22} + (c_{12} + c_{66})u_{1,12} + c_{66}u_{2,11} &= 0 \ . \end{aligned} \tag{29}$$

The boundary integral equations take the same general form as for the Laplace equation, the displacement $u$ and traction $\tau$ playing the roles of potential and flux, respectively. Thus, corresponding to Eq. (1) and Eq. (2) are the displacement and traction equations

$$u_k(P) = \int_\Gamma U_{kj}(P,Q)\,\tau_j(Q)\,dQ - \int_\Gamma T_{kj}(P,Q)\,u_j(Q)\,dQ \tag{30}$$

$$\tau_k(P) = \int_\Gamma S_{kj}(P,Q)\,\tau_j(Q)\,dQ - \int_\Gamma W_{kj}(P,Q)\,u_j(Q)\,dQ \tag{31}$$

(as usual, summation over the repeated index $j$ is implied). The fundamental solution $U_{kj}(P,Q)$ is the displacement field at $Q$ due to a point force at $P$ in an infinite sheet of orthotropic material [78, 79]. This function is given by

$$U_{11}(P,Q) = \frac{1}{\beta}\left[\sqrt{\alpha_1}\,A_2^2\,\log(r_1) - \sqrt{\alpha_2}\,A_1^2\,\log(r_2)\right]$$

$$
\begin{aligned}
U_{12}(P,Q) &= \frac{1}{\beta}\left[A_1\, A_2\,(\theta_2-\theta_1)\right] \\
U_{21}(P,Q) &= U_{12}(P,Q) \\
U_{22}(P,Q) &= \frac{1}{\beta}\left[\frac{A_2^2\,\log(r_2)}{\sqrt{\alpha_2}} - \frac{A_1^2\,\log(r_1)}{\sqrt{\alpha_1}}\right] \quad ,
\end{aligned}
\tag{32}
$$

where the distance and angle functions are given by

$$
r_k^2 = (Q_1-P_1)^2 + \frac{1}{\alpha_k}(Q_2-P_2)^2 \tag{33}
$$

and

$$
\theta_k = \tan^{-1}\left[\frac{Q_2-P_2}{\sqrt{\alpha_k}\,(Q_1-P_1)}\right] \quad . \tag{34}
$$

The constants are defined by

$$
\begin{aligned}
\beta &= 2\pi\,(\alpha_1-\alpha_2)\; s_{22} \\
\alpha_1+\alpha_2 &= \frac{2s_{12}+s_{66}}{s_{22}} \\
\alpha_1\,\alpha_2 &= \frac{s_{11}}{s_{22}} \\
A_k &= s_{12}-\alpha_k\, s_{22}
\end{aligned}
\tag{35}
$$

and

$$
\begin{bmatrix} c_{11} & c_{12} \\ c_{12} & c_{22} \end{bmatrix} = \begin{bmatrix} s_{11} & s_{12} \\ s_{12} & s_{22} \end{bmatrix}^{-1} , \qquad c_{66} = \frac{1}{s_{66}} \quad . \tag{36}
$$

The expressions for the subsequent derivatives $T(P,Q)$, $S(P,Q)$ and $W(P,Q)$, are quite lengthy, and these formulas have consequently been exiled to the appendix.

## 5.2 Singular Integrals

There are several aspects of the orthotropic singular integral analysis that distinguish it from Laplace. Foremost perhaps is that in the limit to the boundary, it is no longer convenient to approach along the normal direction. The approach direction is arbitrary, as long as it is not tangent to the boundary, and for the Laplace kernels a normal limit was chosen to simplify the form of $r^2$: in this case $r^2 = (s-t)^2 + \varepsilon^2$, *i.e.*, there is no first order term. The integrations are quite a bit simpler if this linear term is missing. For the orthotropic analysis, a linear term is avoided by an appropriate non-normal limit direction. Second, as noted above, the kernel functions are more complicated than for Laplace. For computational efficiency of the analysis code, it makes sense to break the integration into its basic components, rather than attempting to provide analytic formulas for a complete kernel function. This somewhat vague statement will be clarified in the discussion of the Maple scripts below. The reader will probably be relieved to hear that the entire analysis of Section 4 will not be repeated – these points can be illustrated by examining the coincident integration for the hypersingular kernel.

In this first section of Maple script note the revised limit direction, where `alpha` will be either $\alpha_1$ of $\alpha_2$ (defined in Eq. (35)), depending upon which term is being integrated:

```
mp[1] := 1-t;
mp[2] := t;
mq[1] := 1-s;
mq[2] := s;
jn[1] := y1-y0;
jn[2] := x0-x1;
p1 := mp[1]*x0 + mp[2]*x1 - eps*jn[1];
p2 := mp[1]*y0 + mp[2]*y1 - eps*alpha*jn[2];
q1 := mq[1]*x0 + mq[2]*x1;
q2 := mq[1]*y0 + mq[2]*y1;
rsq :=  b2*(s-t)^2 + b0*eps^2;
```

The coefficients `b0` and `b2` are once again stand-ins for quantities that can be computed, inserted to simplify the appearance of the formulas. Examining the expressions for $W_{kjL}$ in the appendix, the hypersingular kernel is seen to consist of linear combinations of $r_k^{-2}$ and $r_k^{-4}$ terms, and this next section considers the $r_k^{-2}$ case. It might appear from this script that terms of the form $\varepsilon^{-1}$ are being recklessly thrown away. However, it is easily checked (again, with Maple) that these terms cancel with corresponding ones from the $r_k^{-4}$ part of the kernel. (The $\varepsilon^{-1}$ term did not appear in the Laplace analysis because the two components of the hypersingular kernel were treated together). First the $s$ integration:

```
KW1 := 1/rsq;
for j from 1 to 2 do
z := int(mq[j]*KW1,s=0..1);
z := subs(sqrt(b2*b0*eps^2)=eps*sqrt(b2*b0),z):
z := subs(1/sqrt(b2*b0*eps^2)=1/(eps*sqrt(b2*b0)),z):
z := subs(arctan(
      b2*(-1+t)/eps/sqrt(b2*b0))=-pi/2,z):
z := subs(arctan(
      (b2*t)/eps/sqrt(b2*b0))=pi/2,z):
z := expand(z);
z := subs(1/eps=ee,z);
z := collect(z,ee);
z := coeff(z,ee,0);
z := subs(eps=0,z);
as[j] := z;
od;
```

and then the $t$ integration:

```
for k from 1 to 2 do
 for j from 1 to 2 do
   z := as[j];
   z := int(z*mp[k],t=0..1);
   w1[k,j] := z;
 od;
od;
```

The numerators attached to $r^{-4}$ in $W_{kjL}$ come in three flavors, and this is conveniently handled by defining the array `KW[m]`, $1 \leq$`m`$\leq 3$. This piece of coding is further complicated by the fact that the $t^{-1}$ divergent expression arises here:

```
KW[1] := expand((q1-p1)^2)/(rsq*rsq);
KW[2] := expand((q1-p1)*(q2-p2))/(rsq*rsq);
KW[3] := expand((q2-p2)^2)/(rsq*rsq);
for m from 1 to 3 do
 for j from 1 to 2 do
z := int(mq[j]*KW[m],s=0..1);
z := subs(sqrt(b2*b0*eps^2)=eps*dd,z):
z := subs(1/sqrt(b2*b0*eps^2)=1/(eps*dd),z):
z := subs(arctan(b2*(-1+t)/eps/dd)=-pi/2,z):
z := subs(arctan((b2*t)/eps/dd)=pi/2,z):
z := subs((b2*b0*eps^2)^(3/2)=eps^3*dd^3,z):
z := subs(1/(b2*b0*eps^2)^(3/2)=1/(eps^3*dd^3),z):
z := expand(z);
z := subs(1/eps=ee,z);
z := collect(z,ee);
z := coeff(z,ee,0);
z := subs(eps=0,z);
   ax[j,m] := z;
 od;
od;
for k from 1 to 2 do
 for j from 1 to 2 do
  for m from 1 to 3 do
   z := ax[j,m];
   z := expand(z*mp[k]);
# get rid of 1/t or 1/(1-t)
if j=1 then
  z := subs(1/t=tt,z);
  z := collect(z,tt);
  z := coeff(z,tt,0);
fi;
if j=2 then
  z := subs(t=1-w,z);
  z := expand(z);
  z := subs(1/w=ww,z);
  z := collect(z,ww);
  z := coeff(z,ww,0);
  z := subs(w=1-t,z);
  z := expand(z);
fi;
   z := int(z,t=0..1);
   w2[k,j,m] :=  z;
  od;
```

```
 od;
od;
```

The formulas for `w1[k,j]` and `w2[k,j,m]` are used directly in the fortran coding.

### 5.3 Fracture Calculations

The two plane stress examples to be presented involve a single interior crack, one horizontal, Fig. 5(a), and one inclined at an angle $\phi = 45^o$ with the horizontal Fig. 5(b). The crack has length 2a = 0.4, the plate has height 2H = 2.0 and width 2W = 1.0, and the applied traction is $\tau_a = 10$ MPa. The material properties correspond to average smeared-out properties of fibreglass [80] and are given in terms of the Young's moduli, shear modulus and Poisson's ratio,

$$\begin{aligned} E_1 &= 48.26 \text{ GPA} \\ E_2 &= 17.24 \text{ GPA} \\ \mu_{12} &= 6.89 \text{ GPA} \\ \nu_{12} &= 0.291 \ . \end{aligned} \tag{37}$$

These quantities can be related to the elastic constants [81].

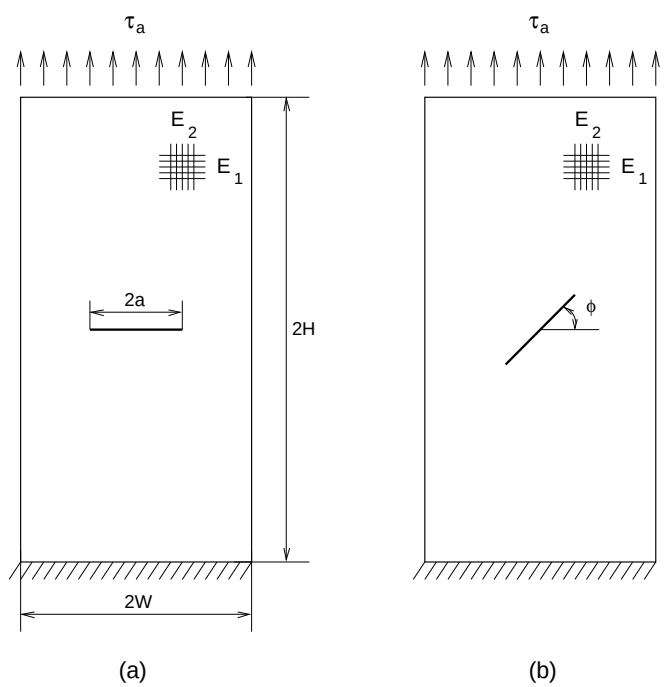


Figure 5: Geometry and boundary conditions for a central crack in a plane orthotropic plate under remote loading. (a) horizontal crack; (b) inclined crack.

The linear element Symmetric-Galerkin solution for these problems has been compared against the finite element solution provided by the program FRANC [82]. The point of comparison is the main quantity of interest in these calculations, the jump in displacement ('displacement discontinuity' or crack opening displacement (COD)) $\Delta\mathbf{u}$ along the crack.

The finite element meshes, and the corresponding solution, are illustrated in Figures 6 and 7. The mesh for the horizontal crack has 768 nodes and 266 quadratic (six-noded triangles, and eight-noded quadrilaterals) elements. The mesh for the inclined crack has 790 nodes and 276 elements. As indicated by the rosette of finite elements around the crack tips, special quarter-point elements are used in the crack tip region.

For the Symmetric-Galerkin calculations, the outer boundary of the plate has been discretized with 60 equal length linear elements. The nodal locations coincide with the FEM boundary discretization. The crack face employs 8 linear boundary elements, with a finer discretization towards the crack tip.

Table 3 shows the COD results for the horizontal crack. Due to symmetry symmetry, the reported results are for the left portion of the crack only. The last column of this table is computed as

$$\Delta u_{\bullet}(\%) = \frac{\Delta u_{\bullet}(\text{FEM}) - \Delta u_{\bullet}(\text{SG-BEM})}{\Delta u_{\bullet}(\text{FEM})} 100\% \tag{38}$$

The CODs obtained are in good agreement, the largest discrepancy being less than 5%. For this problem, the crack sliding displacement should be zero (*i.e.* $\Delta u_x = 0$). The numerical values for both the BEM and FEM are of the order of $10^{-8}$ or less, which indicates that consistent solutions have been obtained.

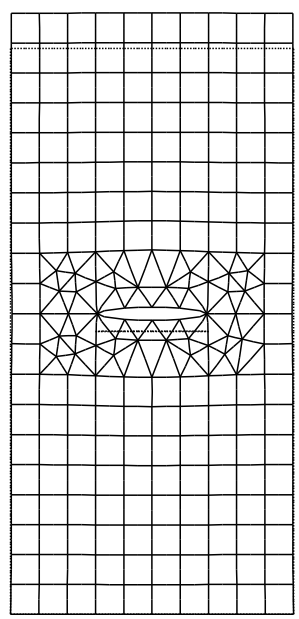

Figure 6: Finite element solution for a central crack in an orthotropic plate under remote tension; solid line denotes the deformed configuration and the dashed line denotes the original configuration.

Tables 4 and 5 show the results for the displacement discontinuity $\Delta \mathbf{u} = (\Delta u_x, \Delta u_y)$ for the inclined crack (Figure 6(b)). As before, the results for $\Delta u_y$ are in good agreement, the largest discrepancy being 5.07%. The results for $\Delta u_x$,

Table 3: Crack Opening Displacement $\Delta u_y$ for the horizontal crack. The solution is for half crack, starting at the left crack tip.

| $x$ | $y$ | SG-BEM $\Delta u_y$ (x$10^{-3}$) | FEM $\Delta u_y$ (x$10^{-3}$) | $\Delta u_y(\%)$ |
|---|---|---|---|---|
| 0.3000 | 1.000 | 0.000000 | 0.000000 | 0.00 |
| 0.325 | 1.000 | 0.227131 | 0.230606 | 1.51 |
| 0.400 | 1.000 | 0.391940 | 0.411062 | 4.65 |
| 0.450 | 1.000 | 0.439092 | 0.460448 | 4.64 |
| 0.500 | 1.000 | 0.453433 | 0.476836 | 4.91 |

however, display a larger discrepancy, especially for the quarter point nodes in the finite element mesh. These nodes are very close to the crack tip and the BEM results, which do not employ a special tip approximation, are consequently sensitive to the numerical discretization. Nevertheless, the actual numerical values for $\Delta u_x$ are of comparable magnitudes. A finer boundary element mesh or an appropriate crack tip treatment in the BEM analysis would probably reduce the difference between the results.

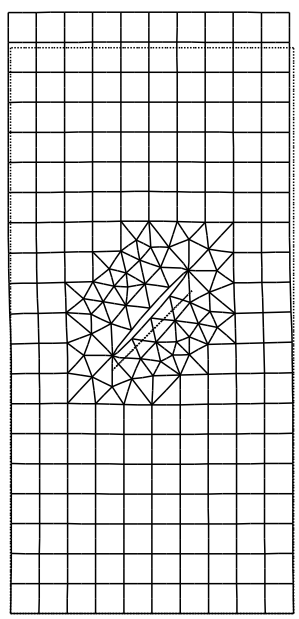

Figure 7: Finite element solution for an inclined crack in an orthotropic plate under remote tension; solid line denotes the deformed configuration and the dashed line denotes the original configuration.

Table 4: Displacement discontinuity $\Delta u_x$ for the inclined crack.

| $x$ | $y$ | $\Delta u_x$(x$10^{-4}$) SG-BEM | $\Delta u_x$(x$10^{-4}$) FEM | $\Delta u_x$(%) |
|---|---|---|---|---|
| 0.3586 | 0.8586 | 0.000000 | 0.000000 | 0.00 |
| 0.3763 | 0.8763 | -0.049903 | -0.065051 | 23.29 |
| 0.4293 | 0.9293 | -0.105063 | -0.113276 | 7.25 |
| 0.4646 | 0.9646 | -0.125796 | -0.139346 | 9.72 |
| 0.5000 | 1.0000 | -0.132743 | -0.145958 | 9.05 |
| 0.5353 | 1.0353 | -0.125730 | -0.139309 | 9.75 |
| 0.5707 | 1.0707 | -0.104960 | -0.113400 | 7.44 |
| 0.6237 | 1.1237 | -0.049838 | -0.064930 | 23.24 |
| 0.6414 | 1.1414 | 0.000000 | 0.000000 | 0.00 |

Table 5: Displacement discontinuity $\Delta u_y$ for the inclined crack.

| $x$ | $y$ | $\Delta u_y$(x$10^{-4}$) SG-BEM | $\Delta u_y$(x$10^{-4}$) FEM | $\Delta u_y$(%) |
|---|---|---|---|---|
| 0.3586 | 0.8586 | 0.000000 | 0.000000 | 0.00 |
| 0.3763 | 0.8763 | 0.163476 | 0.164245 | 0.47 |
| 0.4293 | 0.9293 | 0.283705 | 0.298861 | 5.07 |
| 0.4646 | 0.9646 | 0.318479 | 0.334257 | 4.72 |
| 0.5000 | 1.0000 | 0.329145 | 0.345614 | 4.77 |
| 0.5353 | 1.0353 | 0.318613 | 0.334217 | 4.67 |
| 0.5707 | 1.0707 | 0.283939 | 0.298794 | 4.97 |
| 0.6237 | 1.1237 | 0.163708 | 0.164171 | 0.28 |
| 0.6414 | 1.1414 | 0.000000 | 0.000000 | 0.00 |

## 6 Singular Integrals: Curved Elements

Although it may appear that the techniques described above are inherently limited to the linear element, they are in fact equally applicable to higher order approximations [68]. In the linear interpolation, the simplifications that allow the analytic integration and limit evaluation to go forward are that (a) the distance function $r^2$ is a quadratic polynomial, and (b) the jacobian is a constant. Lacking these properties with a higher order interpolation, the integrands become sufficiently complicated that exact integration is not *immediately* possible. Nevertheless, the singular integrals can be split into two pieces: the singular term will look essentially like a linear element integral, and will therefore be amenable to analytic integration and limit evaluation; the remainder term, although somewhat complicated, will be completely non-singular. Moreover, it will usually be relatively small in value compared to the singular part, and can therefore be treated efficiently by low order numerical quadrature. This section will show how to accomplish this decomposition.

The procedures for a curved element will be described using the Overhauser cubic spline [42], probably the most complicated two-dimensional element that has been used in boundary element analysis. This element takes four consecutive nodes, $\{P_k\}_{k=1}^4$, to define the piece of curve between the second and third nodes $[P_2, P_3]$. The explicit parametric form is

$$Q(t) = \left( \sum_{k=1}^{4} x_k M_k(t), \sum_{k=1}^{4} y_k M_k(t) \right) \ , \tag{39}$$

where $P_k = (x_k, y_k)$ and the shape functions for $0 \le t \le 1$ are

$$\begin{aligned} M_1(t) &= -\left(t - 2t^2 + t^3\right)/2 \\ M_2(t) &= \left(2 - 5t^2 + 3t^3\right)/2 \\ M_3(t) &= \left(t + 4t^2 - 3t^3\right)/2 \\ M_4(t) &= -\left(t^2 - t^3\right)/2 \ . \end{aligned} \tag{40}$$

The motivation for this less than obvious definition is that the corresponding isoparametric approximation for $\phi$,

$$\phi\left(Q(t)\right) = \sum_{1}^{4} \phi(P_k) M_k(t) \ , \tag{41}$$

is differentiable everywhere on the boundary.

To illustrate the splitting into singular and non-singular parts, it suffices to consider the coincident integration, the corresponding treatment of the adjacent case being straightforward. Including the limit to the boundary term, $\mathbf{R} = Q(s) - (P(t) - \varepsilon \mathbf{N}) = (r_1(t,s), r_2(t,s))$ and using Eqs. (39) and (40),

$$\begin{aligned} r_1(t,s) &= a_x(s-t) + b_x(s-t)^2 + g_x(s-t)^3 - \varepsilon N_1 \\ r_2(t,s) &= a_y(s-t) + b_y(s-t)^2 + g_y(s-t)^3 - \varepsilon N_2 \\ r^2 &= \varepsilon^2 + \alpha(s-t)^2 + \beta(s-t)^3 + \cdots \ , \end{aligned} \tag{42}$$

where the polynomial coefficients $\{a, b, g\}$ are given in terms of the nodal coordinates,

$$\begin{aligned} a_x &= (x_3 - x_1)/2 \\ b_x &= (2x_1 - 5x_2 + 4x_3 - x_4)/2 \\ g_x &= (-x_1 + 3x_2 - 3x_3 + x_4)/2 \ , \end{aligned} \tag{43}$$

and expressions for $\alpha$, $\beta$, etc. are easily obtained. In addition, the jacobian is given by

$$J_q(s) = \|\frac{d}{ds}Q(s)\| = \left(j_0 + j_1 s + j_2 s^2\right)^{\frac{1}{2}} \ . \tag{44}$$

With the appearance of a square root in the jacobians, and the high order polynomials in the denominators, analytic integration of the boundary integrals is clearly not possible.

The splitting for $G(P, Q)$ is accomplished by appropriately rewriting each factor in the product $J_q(s)\log(r^2)$. The logarithm is straightforward,

$$\begin{aligned} \log(r^2) &= \log\left(\alpha(s-t)^2 + \beta(s-t)^3 + \cdots\right) \\ &= \log\left(\alpha(s-t)^2\right) + \log\left(1 + \frac{\beta}{\alpha}(s-t) + \cdots\right) \ . \end{aligned} \tag{45}$$

The jacobian is handled as

$$J_q(s) = \hat{J}(s,t) + \left(J_q(s) - \hat{J}(s,t)\right) \tag{46}$$

where $\hat{J}(s,t)$ is a Taylor expansion of $J_q(s)$ expanded around $s = t$, and is therefore a polynomial in $s - t$ [83]. Hence, the partitioning is given by

$$\begin{aligned} J_q(s)\log(r^2) &= \hat{J}(s,t)\log\left(\alpha(s-t)^2\right) + J_q(s)\log\left(1 + \frac{\beta}{\alpha}(s-t) + \cdots\right) \\ &+ \left(J_q(s) - \hat{J}(s,t)\right)\log\left(\alpha(s-t)^2\right) \ . \end{aligned} \tag{47}$$

The first term is simple enough to be integrated exactly *and* it contains *all* of the singularity – the two remainder terms are well behaved and can be safely evaluated numerically.

There remains the question of the order of the Taylor expansion $\hat{J}(s,t)$. The main concern is the integration of the last term in Eq. (47), the remainder in the Taylor series, which is $\mathcal{O}((s-t)^\gamma)$, multiplied by the log singularity. With symbolic computation, it is easy to include any number of terms in $\hat{J}(s,t)$, but for efficiency it is still desirable to limit the complexity of the analytic formulas as much as possible. A three term expansion has been found to be satisfactory if standard Gauss quadrature is used to evaluate this last term. However, a special quadrature technique that specifically accounts for the logarithmic singularity can also be employed [3, 84, 85]. This special Gauss rule is based on observing that

$$\int_0^1 f(t)\log(t)\ dt = -\int_0^1\int_0^1 f(st)\ ds\ dt \ . \tag{48}$$

For well behaved $f(t)$, the non-singular double integral can be evaluated with a simple Gauss rule. If this quadrature method is employed in the integration of Eq. (47), a one term expansion $\hat{J}(s,t) = J_q(t)$ would probably suffice.

For the more singular integrals, $J_p$ appears in the integral of the first derivative of the Green's function, but otherwise the jacobians are absorbed into the respective normals in the kernel function. Thus, the main stumbling block to analytic integration is the presence of rational functions with denominators of the form $r^{2k}$. As with the logarithm, the goal will be to find a modified form of the rational function which is exactly integrable but which nevertheless retains all of the singularity at $t = s$. This is achieved by replacing the $r^{-2k}$ terms with the simpler expression $\hat{r}^{-2k}$,

$$\frac{1}{\hat{r}^{2k}} = \frac{1}{\left(\alpha(s-t)^2 + \varepsilon^2\right)^k} \ . \tag{49}$$

consisting of the first two non-zero terms in $r^2$, Eq. (42). These are the most important terms as $s \to t$, and contain the essence of the singularity. Some algebraic manipulation results in

$$\frac{1}{r^2} = \frac{1}{\hat{r}^2} + \left(\frac{1}{r^2} - \frac{1}{\hat{r}^2}\right) \tag{50}$$

$$= \frac{1}{\hat{r}^2} + \left(\frac{\hat{r}^2 - r^2}{r^2\hat{r}^2}\right) \tag{51}$$

For the term in parenthesis, the lowest order term appearing in the numerator is $(s-t)^3$, and the denominator is essentially $(s-t)^4$. The singularity in this remainder is therefore one degree less than $r^{-2}$, which behaves as $(s-t)^{-2}$. The remainder is, however, still singular, and thus this process is iterated one more time. Replacing $r^{-2}$ on the right by Eq. (51) results in

$$\begin{aligned} \frac{1}{r^2} &= \frac{1}{\hat{r}^2} + \frac{\hat{r}^2 - r^2}{\hat{r}^4} + \frac{(\hat{r}^2 - r^2)^2}{r^2\hat{r}^4} \\ &= \frac{1}{\hat{r}^2} - \frac{\beta(s-t)^3}{\hat{r}^4} + I_0(t,s) \ , \end{aligned} \tag{52}$$

where $I_0(t,s)$ is a rational function which is nonsingular at $t = s$. Thus, one can set $\varepsilon = 0$ in $I_0$ and integrate numerically. As with the linear element, the first two terms in Eq. (52) can be integrated analytically without any difficulty, and the limit $\varepsilon \to 0$ can then be computed.

The $r^{-4}$ term in the hypersingular kernel can be manipulated in the same manner. Thus,

$$\begin{aligned} \frac{1}{r^4} &= \frac{1}{\hat{r}^4} + \left(\frac{\hat{r}^4 - r^4}{r^4\hat{r}^4}\right) \\ &= \frac{1}{\hat{r}^4} + \frac{\hat{r}^4 - r^4}{\hat{r}^8} + \frac{(\hat{r}^4 - r^4)^2}{r^4\hat{r}^8} \\ &= \frac{1}{\hat{r}^4} - 2\frac{\beta(s-t)^3}{\hat{r}^6} + I_1(t,s) \ , \end{aligned} \tag{53}$$

In this case $I_1$ is still singular, of the form $(s-t)^{-2}$, but this will be taken care of by the zero in the numerator at $t = s$. As with the choice of order in the Taylor expansion for the jacobian, the process represented by Eq. (52) or Eq. (53) can be repeated as often as desired. More iterations will make the numerical part as weaker, but also increase the complexity (and hence the eventual computational cost) of the analytic formulas.

These simple techniques allow curved elements to be treated *almost* as easily as the linear element. The two main differences are that numerical integration will always be required, where before complete analytic integration was often possible, and that the analytic integration is more involved (*e.g.*, the $\hat{r}^{-4}$ term in Eq. (52)). Again, with symbolic computation, this additional complication is not a problem.

The basic idea of partitioning integrals into singular and non-singular parts can also be applied to boundary integral formulations involving more complicated fundamental solutions [68]. For example, the Green's function kernels for elastic wave scattering (frequency domain) are defined in terms of Hankel functions $H_m(r)$, or exponentials $e^{ikr}$, in two [86] and three dimensions [70], respectively. For the Hankel function, the singular integral analysis analysis can be carried out by invoking the asymptotic form of the Hankel function as $z \to 0$ [87],

$$H_m^{(1)}(z) \approx -\frac{2i}{\pi}\left\{\frac{(m-1)!}{z^m} - J_m(z)\log\left(\frac{z}{2}\right)\right\} \ , \tag{54}$$

where $J_m$ is the Bessel function of order $m$. Only the leading order term in this expansion is shown, the lower order contributions, $z^{-k}, k < m$, will become regular after multiplication by the appropriate coefficient from the kernel function. However, the integrable logarithm term is displayed, to indicate that this term should be pulled out and handled via the special quadrature discussed above.

For three dimensional analysis, the integration of the exponential can be handled simply by Taylor expansions,

$$e^{ikr} = 1 + ikr - \frac{k^2r^2}{2}\cdots \ . \tag{55}$$

With the techniques presented in this section, the limit definition and analytic integration process can be applied to virtually any boundary integral formulation.

## 7 Surface Derivatives

The 'post-processing' evaluation of surface tangential derivatives is an important topic wherein hypersingular integrals must be confronted, or at the very least, sidestepped. It is therefore expected that the Galerkin approach can successfully address this issue, and this section will argue that this is indeed the case. In potential theory, the *normal* flux is known everywhere from the boundary element solution and the prescribed data, but some applications demand the complete derivative on the surface, *e.g.*, the electric field vector. Employing the unit tangent $\mathbf{T}$ in Eq. (2) instead of the normal $\mathbf{N}$, the tangential component of the electric field can be expressed as

$$\frac{\partial \phi(P)}{\partial \mathbf{T}} = \int_\Gamma \left[ \frac{\partial G}{\partial \mathbf{T}}(P,Q) \frac{\partial \phi}{\partial \mathbf{n}}(Q) - \phi(Q) \frac{\partial^2 G}{\partial \mathbf{T} \partial \mathbf{n}}(P,Q) \right] dQ \ , \tag{56}$$

and the expression on the right involves only known quantities. However, the kernel $\partial^2 G / \partial \mathbf{T} \partial \mathbf{N}$ is hypersingular, and the $C^1$ condition once again makes direct evaluation of *nodal* tangential derivative values quite difficult.

The existing methods for evaluating surface derivatives, mostly formulated in terms of computing the surface stress tensor in elasticity, fall into three categories. The initial efforts employed finite differencing [88, 89] or differentiation of the shape functions [90]. These techniques are simple but not highly accurate. A second avenue is to directly collocate the hypersingular integral at the nodes, employing the required $C^1$ elements [91]. As noted in the introduction, these elements are not easy to work with, especially in three dimensions, and boundary corners cannot be easily handled [92].

The third class of methods evaluates the derivatives indirectly, bypassing the differentiability condition. A non-conforming approach computes tangential derivatives at points interior to the element [93, 94, 95], where all functions are differentiable, and the hypersingular integral therefore exists. Nodal values, however, must then be obtained by interpolation, which adds another approximation and, moreover, is not a trivial task in three dimensions. A completely non-hypersingular scheme for calculating nodal values is the 'displacement gradient' approach of Okada *et al.* [54, 96]. This technique develops a non-hypersingular boundary integral equation for the gradient, from which the stress can be computed. Standard numerical methods can be employed [97], but a completely new boundary integral formulation, *i.e.*, new kernel functions, must be implemented and solved.

A general algorithm for direct evaluation of nodal surface derivatives, with continuous ($C^0$) elements, can be based upon the Galerkin approximation [55]. In Galerkin form, Eq. (56) becomes

$$\int_\Gamma \psi_k(P) \frac{\partial \phi(P)}{\partial \mathbf{T}} dP = \tag{57}$$
$$\int_\Gamma \psi_k(P) \int_\Gamma \left[ \frac{\partial G}{\partial \mathbf{T}}(P,Q) \frac{\partial \phi}{\partial \mathbf{n}}(Q) - \phi(Q) \frac{\partial^2 G}{\partial \mathbf{T} \partial \mathbf{n}}(P,Q) \right] dQ \, dP \ .$$

As with the displacement gradient method, this results in a system of algebraic equations for the derivative values everywhere on the boundary: the equation centered at a particular node $P_0$ ($\psi_k(P_0) = 1$) will necessarily involve unknown tangential derivative values at all neighboring nodes (on elements where $\psi_k(P_0) \neq 0$). However, unlike displacement gradient, Eq. (57) decouples at boundary corners. This follows from the fact that the Galerkin weight functions $\psi_k$ at a corner can be chosen to be non-zero only on one side of the corner [67]. In applications which only require the tangential derivative on a segment of the boundary, this can lead to significant savings.

The coefficient matrix, stemming from the left-hand side of Eq. (57), is trivial to compute: it is symmetric, involves only 'nearest neighbor interactions', and the non-zero matrix elements simply require the integration of a pair of shape

functions. Although the evaluation of the right hand side of Eq. (57) will be a relatively expensive calculation, the symmetry of the kernels functions can be invoked to lessen the computation time.

### 7.1 Example Calculations

It is expected that, by now, the reader is tired of looking at Maple codes. Fortunately, the singular integral evaluation for Eq. (57) provides no new challenges, and can be accomplished with the techniques presented in Section 4. We therefore dispense with a singular integral analysis, and immediately present the results from two simple test calculations. More realistic problems will be discussed in the next section. Aside from demonstrating that the method works, the main points of interest are the accuracy of the results, and the ability to handle multiple tangential derivative values at corners.

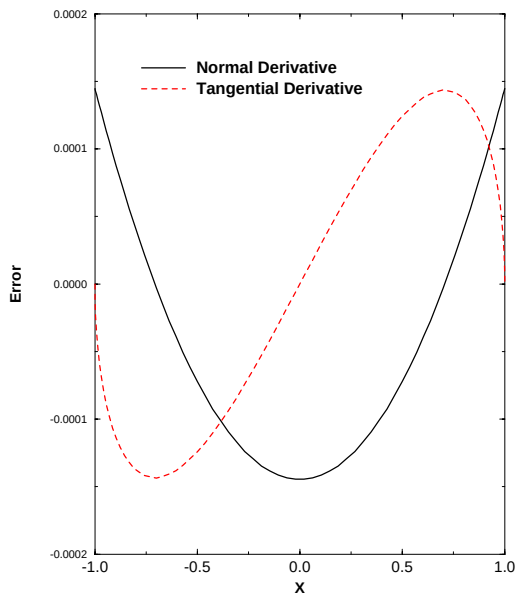


Figure 8: Errors in the calculated normal and tangential components of $\nabla\phi$ for $\mathcal{D}$ the unit disk.

As the first example, consider the Laplace equation posed on the unit disk, with Dirichlet boundary values $\phi = x^2 - y^2$. Fig. 8 displays the errors in the computed normal and tangential derivatives, employing 80 linear elements. The results for the bottom half of the circle are shown, the results for the top being the same. Note that the error in the tangential component is the same order of magnitude as the error in the initial solution.

The second example solves the same Dirichlet problem, but now on the unit square (employing a uniform grid spacing of 0.05). As mentioned in the introduction, previous methods for evaluating surface derivatives have serious difficulties boundary corners and edges. For direct collocation of a hypersingular integral at a corner point, the interpolation of the potential *and* the normal flux be consistent [56, 98], and it is non-trivial to incorporate this constraint in the approximation [57]. It is possible that the 'displacement gradient' method can compute values

at a corner, but existing implementations appear to be valid only for smooth surfaces [54, pg. 789].

| corner point | Normal Derivative Calculated | Normal Derivative Exact | Tangential Derivative Calculated | Tangential Derivative Exact |
|---|---|---|---|---|
| $(0.0^+,\ 0.0)$ | 0.03458 | 0.00000 | 0.01488 | 0.00000 |
| $(0.0,\ 0.0^+)$ | −0.03458 | 0.00000 | 0.01488 | 0.00000 |
| $(1.0^-,\ 0.0)$ | 0.03376 | 0.00000 | 1.98500 | 2.00000 |
| $(1.0,\ 0.0^+)$ | 1.96531 | 2.00000 | −0.01467 | 0.00000 |
| $(1.0,\ 1.0^-)$ | 1.96613 | 2.00000 | −1.98521 | −2.00000 |
| $(1.0^-,\ 1.0)$ | −1.96613 | −2.00000 | −1.98521 | −2.00000 |
| $(0.0^+,\ 1.0)$ | −1.96531 | −2.00000 | −0.01467 | 0.00000 |
| $(0.0,\ 1.0^-)$ | −0.03376 | 0.00000 | 1.98500 | 2.00000 |

Table 6: Calculated normal and tangential derivatives at the corners of the unit square. The boundary values are $\phi = x^2 - y^2$.

The flexibility provided by the choice of weight function allows a simple treatment of corners within the Galerkin method [67]. In two dimensions, the corner is represented by the usual technique of a 'double node' pair, one node for each side of the corner. A tangential derivative equation for each node is obtained by specifying that the weight function $\psi_k$ be non-zero on only one side of the corner. Thus, the two corner nodes have different, non-overlapping, weight functions. As a consequence the tangential derivative equations 'terminate' at a corner: the product of the two shape functions at the corner is zero, and thus there is no matrix element connecting the two tangential derivative values. For applications which do not require knowledge of the derivative everywhere on the boundary, this is potentially very useful.

The calculated values for both normal and tangential derivatives at the corners of the square are shown in Table 7.1. The multiple values at the corners are accurately represented. It is possibly surprising that the tangential values in this case are more accurate than the computed normal derivative. However, this is apparently not uncommon [93].

# 8 Application: Electromigration

As an application of the techniques presented above, we consider the modeling of electromigration, void motion in aluminum thin film interconnects in microelectronic devices. Open-circuit failure due to electromigration is one of the most serious reliability problems in integrated circuits [99, 100, 101]. Void nucleation occurs during thin film thermal processing, and subsequent void migration takes place during circuit operation. External forces, such as mechanical loads and thermal stresses can affect void motion, but herein we will only consider the interaction of the void with an imposed electric field.

The electric field interacts with the void through its tangential component on the void surface. A Neumann boundary value problem for the electrostatic potential $\Phi$ must first be solved, and then $\mathbf{E} \bullet \mathbf{T} = -\nabla\Phi \bullet \mathbf{T}$ must be computed.

The geometry for a two dimensional simulation of electromigration-induced void dynamics is shown in Fig. 9. The domain $\mathcal{D}$ is a strip, $-\infty < x < \infty$, $0 \leq y \leq W$, representing an aluminum thin film which has been damaged by the formation of a void. The boundary conditions are zero normal flux on the insulating strip boundaries and on the void surface, together with an imposed electric field $\mathbf{E} = (E_\infty, 0)$ at infinity, *i.e.*, far away from the void surface. It is convenient to reformulate the problem by defining the potential $\phi$ via

$$\Phi = -E_\infty x + \phi \ , \tag{58}$$

so that $\phi$ vanishes at infinity. Note that the boundary conditions for $\phi$ remain zero normal flux on the strip boundaries, where $n = (n_x, n_y) = (0, \pm 1)$, while on the void surface

$$\nabla\phi \bullet n = E_\infty n_x \ . \tag{59}$$

The electric field contribution to the flux of atoms on the void surface is proportional to the tangential component, $E_s = \nabla\Phi \bullet \mathbf{T} = \nabla\phi \bullet \mathbf{T} - E_\infty t_x$, where $\mathbf{T} = (t_x, t_y)$ is the unit tangent vector on the void. Once the surface atomic flux is known, the void velocity normal to the void surface can be computed from the surface divergence, $dE_s/ds$, where $ds$ indicates an arclength derivative [99, 102, 101]. The void surface can then be advanced in time, and the process repeated with the new geometry. The calculations below were employed in determining steady state void morphologies, and thus computing $E_s$ sufficed. The derivative $dE_s/ds$ can be computed using the same techniques [103].

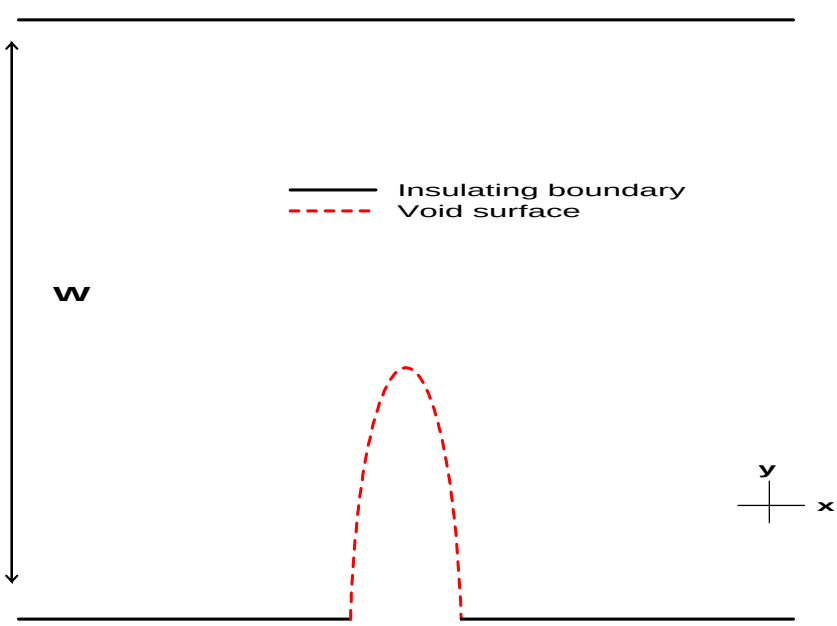


Figure 9: A two dimensional model for a damaged interconnect film, consisting of a strip of infinite length and width $W$ (solid line) containing a void defect (dashed line).

The boundary integral solution for $\phi$ is obtained using a linear element symmetric Galerkin approximation. As the boundary condition on the void is speci-

fied flux, only the flux equation, Eq. (2), is required. The results of the boundary element tangential derivative calculations are compared to corresponding computations carried out with the finite element method (FEM). The FEM meshes were graded very finely near the void surface where high potential gradients were expected, and along the void surface for accurate evaluation of the tangential component of $\mathbf{E}$. Typically, the number of degrees of freedom involved in the FEM simulations is on the order of $10^4$. In the BEM calculations discussed below, the number of nodes on the void is 101. This was the only surface modeled, the boundary conditions on the interconnect being incorporated (approximately) into the Green's function. Further details on the BEM and FEM solution procedures can be found in [55].

The tangential derivative solutions for an initial void shape and three perturbations of this shape, shown in Fig. 10, are displayed in Fig. 11. The initial shape is a circular arc, the steady state solution for $E_\infty = 0$, while the other three void morphologies are steady state solutions for increasing $E_\infty$. In this first set of calculations the width of the interconnect is $W = 3.0$, and thus the void is well separated from the top boundary. The results in Fig. 11 are in excellent agreement with the finite element solutions.

A second set of steady state void morphologies and the corresponding void surface solutions for the tangential component of $\mathbf{E}$ are displayed in Figs. 12 and 13. The width of the strip has been reduced to $W = 0.5$, and thus the void spans roughly 80% of the interconnect in the $y$ direction. For such geometries, the electric field computation becomes more difficult for both finite element and boundary element methods. The magnitude of the electric field near the top of the void is much higher and the electric field gradients are much steeper. Once again, the results from both methods match very well.

# 9 Conclusions

Hybrid analytical/numerical algorithms for the evaluation of singular Galerkin boundary integrals have been presented. We have tried to argue that singular integration for the Galerkin method is **not** the beast that it appears to be. The limit to the boundary provides a mathematically sound and physically sensible definition of the singular and hypersingular integrals, and leads to a direct, and completely general, evaluation algorithm. In our opinion, this is much simpler, conceptually and computationally, than 'regularizing' a non-existent integral (*e.g.*, an 'exclusion zone' analysis). The task of carrying out the analytic integrations and the limit process, admittedly onerous by hand, is conveniently automated with symbolic computation.

One final advertisement for symbolic manipulation: once the procedures have been worked out for one equation, it is relatively easy to modify the Maple scripts to generate the needed formulas for another equation. This is due to the fact that the nature of the corresponding kernel singularities is, in all cases, identical. Thus, in creating the orthotropic code, the existence of the Laplace scripts was exploited to considerably shorten the development time.

The important issue of efficiency was not addressed herein, but previous

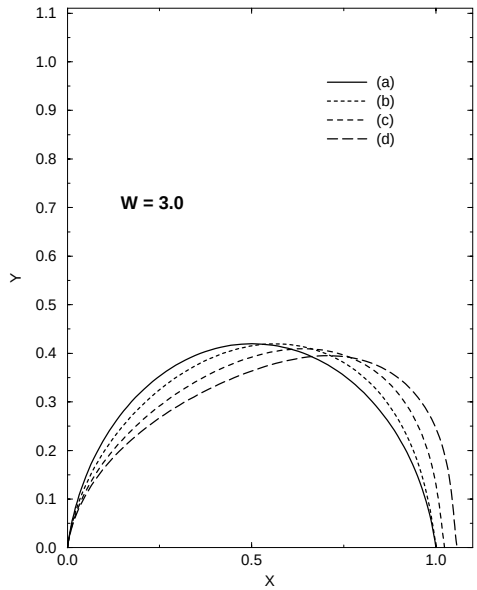


Figure 10: Four steady state void shapes for different applied field $E_\infty$ in an Al strip of width $W = 3.0$.

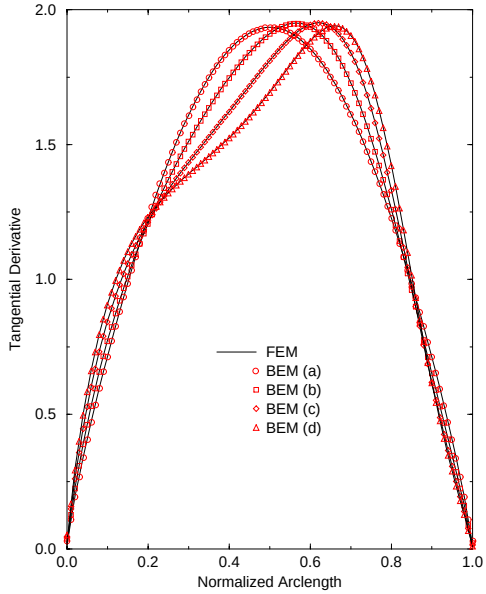


Figure 11: Comparison between the tangential derivative calculations using the FEM and BEM methods for the voids shown in Fig. 10.

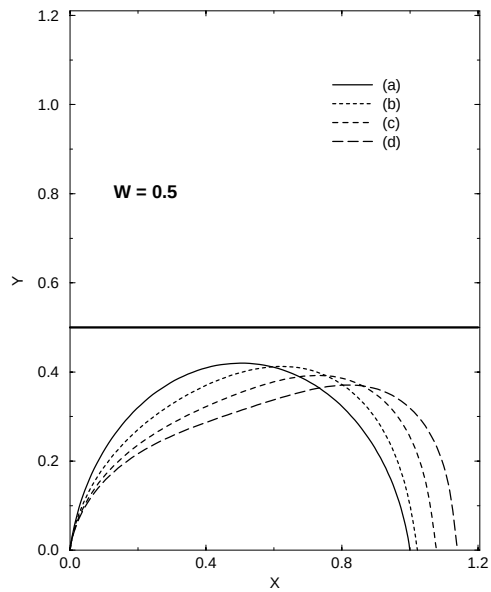


Figure 12: Four steady state void shapes in an Al strip of width $W = 0.5$.

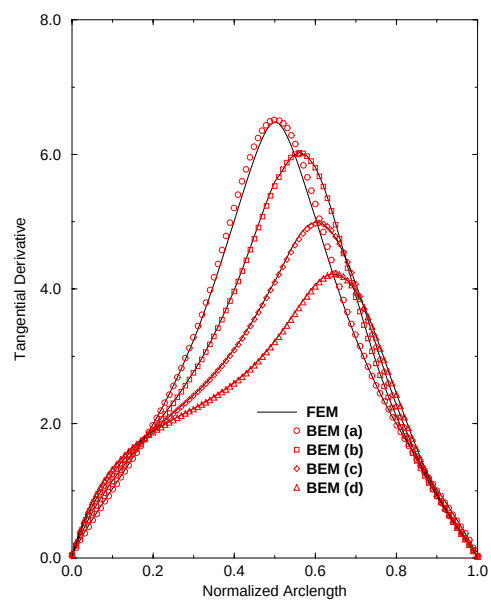


Figure 13: Comparison between the tangential derivative calculations using the FEM and BEM methods for the voids shown in Fig. 12.

work [13, 53] has established that the hybrid algorithms are much faster than a brute force numerical approach. These efficient methods, added to the significant computational advantages provided by symmetry, create a fast Symmetric-Galerkin algorithm. With the other principal virtues of Galerkin – accuracy, hypersingular analysis with standard $C^0$ interpolation, and a reliable corner treatment – Symmetric-Galerkin becomes a highly attractive general purpose algorithm for boundary integral analysis.

The Galerkin approach was also shown to be very useful for the evaluation of surface tangential derivatives. The primary advantages over previous methods are essentially the same as those listed above: accurate *nodal* derivative values are obtained with $C^0$ interpolation, and the method is efficient – stress components can be calculated directly, and the system of equations naturally terminates at boundary corners. Moreover, multiple values at corners can be accurately reproduced.

For those who are interested, the author intends to make the symbolic computation programs discussed herein available over the internet. The home page *www.epm.ornl.gov/~gray* contains a link to Symmetric-Galerkin material, and it is hoped that the Maple scripts will eventually be found there.

## Acknowledgments

This research was supported by the Applied Mathematical Sciences Research Program of the Office of Mathematical, Information, and Computational Sciences, U.S. Department of Energy, under contract DE-AC05-96OR22464 with Lockheed Martin Energy Research Corp. Additional support from the National Science Foundation under grant PHY94-07194 with the Institute for Theoretical Physics, University of California, Santa Barbara, and from the Department of Civil and Environmental Engineering, University of California, Davis, is also gratefully acknowledged. G. H. Paulino prepared some of the figures and provided many valuable suggestions for improving the manuscript. The author would also like to thank P. A. Wawrzynek, D. Maroudas, and M. Enmark for their assistance.

### Appendix: Kernels for Orthotropic Elasticity

The formulas for the traction fundamental solution $T_{kj}(P,Q)$ in the displacement equation, and the tensors $S_{kjL} = U_{kj,L}$ and $W_{kjL} = T_{kj,L}$ for the traction equation are presented below.

**Tensor** $T_{kj}$

$$
\begin{aligned}
T_{11}(P,Q) &= \frac{1}{\beta}\,\mathbf{n}\bullet\mathbf{R}\left(\frac{A_1}{\sqrt{\alpha_2}\,r_2^2} - \frac{A_2}{\sqrt{\alpha_1}\,r_1^2}\right) \\
T_{12}(P,Q) &= \frac{1}{\beta}\left(\frac{M_1\,A_2}{r_1^2} - \frac{M_2\,A_1}{r_2^2}\right) \\
T_{21}(P,Q) &= \frac{1}{\beta}\left(\frac{M_1\,A_1}{\alpha_1\,r_1^2} - \frac{M_2\,A_2}{\alpha_2\,r_2^2}\right)
\end{aligned}
\tag{60}
$$

$$T_{22}(P,Q) \quad = \quad \frac{1}{\beta}\,\mathbf{n}\bullet\mathbf{R}\left(\frac{A_1}{\sqrt{\alpha_1}\,r_1^2} \;-\; \frac{A_2}{\sqrt{\alpha_2}\,r_2^2}\right) \tag{61}$$

Here $\mathbf{R} = Q - P$, $\mathbf{n} = \mathbf{n}(Q)$ is the unit normal vector at $Q$, and the parameters $M_k$ are

$$M_k = \sqrt{\alpha_k}\,n_y\,(Q_1 - P_1) - \frac{n_x}{\sqrt{\alpha_k}}\,(Q_2 - P_2) \tag{62}$$

For a point $P$ interior to the domain, the displacement equation Eq. (30) can be differentiated with respect to $P$, the derivative moved underneath the integral sign, resulting in

$$u_{k,L}(P) \equiv \int_\Gamma S_{kjL}(P,Q)\,\tau_j(Q)\,dQ - \int_\Gamma W_{kjL}(P,Q)\,u_j(Q)\,dQ \quad . \tag{63}$$

where

$$S_{kjL} = U_{kj,L} \qquad \text{and} \qquad W_{kjL} = T_{kj,L}\ . \tag{64}$$

The formulas for the kernel functions $S_{kjL}$ and $W_{kjL}$ are presented below. The desired integral equations for surface traction or surface stress can be formed by combining the equations for displacement derivatives according to Eq. (28), and thus the full kernels are appropriate linear combinations of $S_{kjL}$ and $W_{kjL}$.

**Tensor** $S_{kjL} = U_{kj,L}$

$$\begin{aligned}
S_{111} &= \frac{1}{\beta}\left[-\frac{\sqrt{\alpha_1}\,A_2^2\,(\,Q_1 - P_1\,)}{r_1{}^2} + \frac{\sqrt{\alpha_2}\,A_1^2\,(\,Q_1 - P_1\,)}{r_2{}^2}\right] \\
S_{112} &= \frac{1}{\beta}\left[-\frac{A_2^2\,(\,Q_2 - P_2\,)}{\sqrt{\alpha_1}\,r_1{}^2} + \frac{A_1^2\,(\,Q_2 - P_2\,)}{\sqrt{\alpha_2}\,r_2{}^2}\right] \\
S_{121} &= \frac{1}{\beta}\left[-\frac{(\,Q_2 - P_2\,)\,A_2\,A_1}{\sqrt{\alpha_1}\,r_1{}^2} + \frac{(\,Q_2 - P_2\,)\,A_2\,A_1}{\sqrt{\alpha_2}\,r_2{}^2}\right] \\
S_{122} &= \frac{1}{\beta}\left[\frac{(\,Q_1 - P_1\,)\,A_2\,A_1}{\sqrt{\alpha_1}\,r_1{}^2} - \frac{(\,Q_1 - P_1\,)\,A_2\,A_1}{\sqrt{\alpha_2}\,r_2{}^2}\right] \\
S_{211} &= S_{121} \\
S_{212} &= S_{122} \\
S_{221} &= \frac{1}{\beta}\left[\frac{A_1^2\,(\,Q_1 - P_1\,)}{\sqrt{\alpha_1}\,r_1{}^2} - \frac{A_2^2\,(\,Q_1 - P_1\,)}{\sqrt{\alpha_2}\,r_2{}^2}\right] \\
S_{222} &= \frac{1}{\beta}\left[\frac{A_1^2\,(\,Q_2 - P_2\,)}{\alpha_1{}^{3/2}\,r_1{}^2} - \frac{A_2^2\,(\,Q_2 - P_2\,)}{\alpha_2{}^{3/2}\,r_2{}^2}\right]
\end{aligned}$$

**Tensor** $W_{kjL} = T_{kj,L}$

All expressions should be multiplied by $1/\beta$, where $\beta$ is defined in Eq. (35).

$$
\begin{aligned}
W_{111} &= \frac{n_x\, A_2}{\sqrt{\alpha_1}\, r_1{}^2} - \frac{n_x\, A_1}{\sqrt{\alpha_2}\, r_2{}^2} + 2\, \mathbf{n}\bullet\mathbf{R}\,(\,Q_1 - P_1)\left[\frac{A_1}{\sqrt{\alpha_2}\, r_2{}^4} - \frac{A_2}{\sqrt{\alpha_1}\, r_1{}^4}\right] \\
W_{112} &= \frac{n_y\, A_2}{\sqrt{\alpha_1}\, r_1{}^2} - \frac{n_y\, A_1}{\sqrt{\alpha_2}\, r_2{}^2} + 2\, \mathbf{n}\bullet\mathbf{R}\,(\,Q_2 - P_2)\left[\frac{A_1}{\alpha_2{}^{3/2}\, r_2{}^4} - \frac{A_2}{\alpha_1{}^{3/2}\, r_1{}^4}\right] \\
W_{121} &= -\frac{\sqrt{\alpha_1}\, n_y\, A_2}{r_1{}^2} + \frac{\sqrt{\alpha_2}\, n_y\, A_1}{r_2{}^2} + 2\,(\,Q_1 - P_1)\left[-\frac{F_2\, A_1}{r_2{}^4} + \frac{F_1\, A_2}{r_1{}^4}\right] \\
W_{122} &= \frac{n_x\, A_2}{\sqrt{\alpha_1}\, r_1{}^2} - \frac{n_x\, A_1}{\sqrt{\alpha_2}\, r_2{}^2} + 2\,(\,Q_2 - P_2)\left[-\frac{F_2\, A_1}{\alpha_2\, r_2{}^4} + \frac{F_1\, A_2}{\alpha_1\, r_1{}^4}\right] \\
W_{211} &= -\frac{n_y\, A_1}{\sqrt{\alpha_1}\, r_1{}^2} + \frac{n_y\, A_2}{\sqrt{\alpha_2}\, r_2{}^2} + 2\,(\,Q_1 - P_1)\left[\frac{F_1\, A_1}{\alpha_1\, r_1{}^4} - \frac{F_2\, A_2}{\alpha_2\, r_2{}^4}\right] \\
W_{212} &= \frac{n_x\, A_1}{\alpha_1{}^{3/2}\, r_1{}^2} - \frac{n_x\, A_2}{\alpha_2{}^{3/2}\, r_2{}^2} + 2\,(\,Q_2 - P_2)\left[\frac{F_1\, A_1}{\alpha_1{}^2\, r_1{}^4} - \frac{F_2\, A_2}{\alpha_2{}^2\, r_2{}^4}\right] \\
W_{221} &= -\frac{n_x\, A_1}{\sqrt{\alpha_1}\, r_1{}^2} + \frac{n_x\, A_2}{\sqrt{\alpha_2}\, r_2{}^2} + 2\, \mathbf{n}\bullet\mathbf{R}\,(\,Q_1 - P_1)\left[\frac{A_1}{\sqrt{\alpha_1}\, r_1{}^4} - \frac{A_2}{\sqrt{\alpha_2}\, r_2{}^4}\right] \\
W_{222} &= -\frac{n_y\, A_1}{\sqrt{\alpha_1}\, r_1{}^2} + \frac{n_y\, A_2}{\sqrt{\alpha_2}\, r_2{}^2} + 2\, \mathbf{n}\bullet\mathbf{R}\,(\,Q_2 - P_2)\left[\frac{A_1}{\alpha_1{}^{3/2}\, r_1{}^4} - \frac{A_2}{\alpha_2{}^{3/2}\, r_2{}^4}\right]
\end{aligned}
$$

The parameters $F_i$ $(i = 1, 2)$ are

$$
\begin{aligned}
F_1 &= \sqrt{\alpha_1}\, n_y\,(\,Q_1 - P_1\,) - \frac{n_x\,(\,Q_2 - P_2\,)}{\sqrt{\alpha_1}} \\
F_2 &= \sqrt{\alpha_2}\, n_y\,(\,Q_1 - P_1\,) - \frac{n_x\,(\,Q_2 - P_2\,)}{\sqrt{\alpha_2}}
\end{aligned}
$$

and

$$
\mathbf{n}\bullet\mathbf{R} = n_x\,(\,Q_1 - P_1\,) + n_y\,(\,Q_2 - P_2\,)
$$

# References


[1] A. H. Schatz, V. Thomée, and W. L. Wendland. *Mathematical Theory of Finite and Boundary Element Methods.* Birkhäuser, Basel, Boston, & Berlin, 1990.

[2] P. K. Banerjee. *The Boundary Element Methods in Engineering.* McGraw Hill, London, 1994.

[3] A. A. Becker. *The Boundary Element Method in Engineering.* McGraw Hill, New York, 1992.

[4] C. A. Brebbia, J. C. F. Telles, and L. C. Wrobel. *Boundary Element Techniques.* Springer-Verlag, Berlin and New York, 1984.

[5] J. H. Kane. *Boundary Element Analysis in Engineering Continuum Mechanics.* Prentice Hall, New Jersey, 1994.

[6] G. Krishnasamy, F. J. Rizzo, and T. J. Rudolphi. Hypersingular boundary integral equations: Their occurrence, interpretation, regularization and computation. In P. K. Banerjee and S. Kobayashi, editors, *Developments in Boundary Element Methods - Advanced Dynamic Analysis*, volume 7, chapter 7. Elsevier Applied Science Publishers, 1991.

[7] S. L. Crouch and A. M. Starfield. *Boundary Element Methods in Solid Mechanics*. George Allen and Unwin, London, 1983.

[8] T. A. Cruse. *Boundary Element Analysis in Computational Fracture Mechanics*. Kluwer Academic Publishers, Boston, 1988.

[9] S. Mukherjee. *Boundary Element Methods in Creep and Fracture*. Elsevier Applied Science Publishers, England, 1982.

[10] F. Hartmann, C. Katz, and B. Protopsaltis. Boundary elements and symmetry. *Ingenieur-Archiv*, 55:440–449, 1985.

[11] G. Maier, G. Novati, and S. Sirtori. On symmetrization in boundary element elastic and elastoplastic analysis. In G. Kuhn and H. Mang, editors, *Discretization methods in structural mechanics*, pages 191–200. Springer-Verlag, Berlin and New York, 1990.

[12] G. Maier and C. Polizzotto. A Galerkin approach to boundary element elastoplastic analysis. *Computer Methods in Applied Mechanics and Engineering*, 60:175–194, 1987.

[13] C. Balakrishna, L. J. Gray, and J. H. Kane. Efficient analytical integration of symmetric Galerkin boundary integrals over curved elements; thermal conduction formulation. *Comput. Methods Appl. Mech. Engrg.*, 111:335–355, 1994.

[14] S. L. Crouch. Solution of plane elasticity problems by the displacement discontinuity method. *Int. J. Numer. Meth. Engrg.*, 10:301–343, 1976.

[15] N. I. Ioakimidis. A natural approach to the introduction of finite-part integrals into crack problems of three-dimensional elasticity. *Engng. Fract. Mech.*, 16:669–673, 1982.

[16] L. J. Gray, Luiz F. Martha, and A. R. Ingraffea. Hypersingular integrals in boundary element fracture analysis. *Int. J. Numer. Meth. Engrg.*, 29:1135–1158, 1990.

[17] H. K. Hong and J. T. Chen. Derivation of integral equations in elasticity. *J. ASCE, Eng. Mech. Div.*, 114:1028–1044, 1988.

[18] S. Guimarães and J. C. F. Telles. On the hyper-singular boundary-element formulation for fracture-mechanics applications. *Engineering Analysis with Boundary Elements*, 13(4):353–363, 1994.

[19] A. Portela, M. H. Aliabadi, and D. P. Rooke. Dual boundary element method: efficient implementation for cracked problems. *Int. J. Numer. Meth. Engrg.*, 33:1269–1287, 1992.

[20] Q. Huang and T. A. Cruse. On the nonsingular traction-BIE in elasticity. *Int. J. Numer. Meth. Engrg.*, 37:2041–2072, 1994.

[21] E. Siebritz and S. L. Crouch. Two-dimensional elastodynamic displacement discontinuity method. *Int. J. Numer. Meth. Engrg.*, 37(19):3229–3250, 1994.

[22] L. J. Gray, C. Balakrishna, and J. H. Kane. Symmetric Galerkin boundary integral fracture analysis. *Engrg. Analy. Boundary Elements*, 15:103–109, 1995.

[23] M. H. Aliabadi. Boundary element formulations in fracture mechanics. *Appl. Mech. Reviews*, 50(2):83–96, 1997.

[24] C. Chang and M. Mear. Boundary element method for two-dimensional linear elastic fracture analysis. *Int. J. Fracture*, 74:219–251, 1995.

[25] G. Xu and M. Ortiz. A variational boundary integral method for the analysis of 3-D cracks of arbitrary geometry modelled as continuous distributions of dislocation loops. *Int. J. Numer. Meth. Engrg.*, 36:1–27, 1993.

[26] L. J. Gray. Boundary element method for regions with thin internal cavities. *Engrg. Analy. Boundary Elem.*, 6:180–184, 1989.

[27] M. Guiggiani, G. Krishnasamy, T. J. Rudolphi, and F. J. Rizzo. A general algorithm for the numerical solution of hypersingular boundary integral equations. *ASME J. Appl. Mech.*, 59:604–614, 1992.

[28] C.-Y. Hui and S. Mukherjee. Evaluation of hypersingular integrals in the boundary element method by complex variable techniques. *Int. J. Solids Structures.* (in press).

[29] A. M. Linkov and S. G. Mogilevskaya. Complex hypersingular integrals and integral equations in plane elasticity. *Acta Mechanica*, 105:189–205, 1994.

[30] V. Mantič. On computing boundary limiting values of boundary integrals with strongly singular and hypersingular kernels in 3D BEM for elastostatics. *Engineering Analysis with Boundary Elements*, 13:115–134, 1994.

[31] V. Mantič and F. Paris. Existence and evaluation of the two free terms in the hypersingular boundary integral equation of potential theory. *Engineering Analysis with Boundary Elements.* (in press).

[32] D. Rosen and D. E. Cormack. The continuation approach: A general framework for the analysis and evaluation of singular and near-singular integrals. *SIAM J. Appl. Math.*, 55(3):723–762, 1995.

[33] E. D. Lutz, L. J. Gray, and A. R. Ingraffea. An overview of integration methods for hypersingular boundary integrals. In C. A. Brebbia, editor, *Proceedings of the BEM-13 Conference*, Southampton, 1991. Computational Mechanics.

[34] M. Tanaka, V. Sladek, and J. Sladek. Regularization techniques applied to boundary element methods. *Applied Mechanics Reviews*, 47(10):457–499, 1994.

[35] L. J. Gray. Evaluation of hypersingular integrals in the boundary element method. *Mathematical and Computer Modelling*, 15(3-5):165–174, 1991.

[36] P. A. Martin and F. J. Rizzo. On boundary integral equations for crack problems. *Proc. R. Soc. Lond., A*, 421:341–355, 1989.

[37] G. Krishnasamy, F. J. Rizzo, and T. J. Rudolphi. Continuity requirements for density functions in the boundary integral equation method. *Computational Mechanics*, 9:267–284, 1992.

[38] P. A. Martin and F. J. Rizzo. Hypersingular integrals: how smooth must the density be? *Int. J. Numer. Meth. Engrg.*, 39:687–704, 1996.

[39] J. D. Richardson, T. A. Cruse, and Q. Huang. On the validity of conforming BEM algorithms for hypersingular boundary integral equations. *Computational Mechanics*. (in press).

[40] T. A. Cruse and J. D. Richardson. Non-singular Somigliana stress identitites in elasticity. *Int. J. Numer. Meth. Engrg.*, 39(19):3273–3304, 1996.

[41] P. A. Martin, F. J. Rizzo, and T. A. Cruse. Smoothness-relaxation strategies for singular and hypersingular integral equations. (submitted).

[42] C. V. Camp and G. S. Gipson. Overhauser elements in boundary element analysis. *Mathematical and Computer Modelling*, 15(3-5):59–69, 1991.

[43] W. S. Hall and T. T. Hibbs. The treatment of singularities and the application of the $C^1$ Overhauser continuous quadrilateral boundary element to three dimensional elastostatics. In T. A. Cruse, editor, *Advanced Boundary Element Methods*, volume 16, pages 135–144, Berlin and New York, 1988. Springer-Verlag.

[44] Y. J. Liu and F. J. Rizzo. Application of Overhauser $C^1$ continuous boundary elements to hypersingular BIE for 3-d acoustic wave problems. In *Proc. of the Boundary Element 13 Conference*, Southampton, 1991. Computational Mechanics Publications.

[45] J. F. Durodola and R. T. Fenner. Overhauser triangular elements for three dimensional potential problems using boundary element methods. *Int. J. Numer. Meth. Engrg.*, 39(24):4183–4198, 1996.

[46] J. O. Watson. Hermitian cubic and singular elements for plain strain. In P. K. Banerjee and J. O. Watson, editors, *Developments in Boundary Element Methods - Vol. 4*, chapter 1, pages 1–28. Elsevier Applied Science Publishers, London and New York, 1986.

[47] T. J. Rudolphi and K. H. Muci-Küchler. Consistent regularization of both kernels in hypersingular integral equations. In C. A. Brebbia and G. S. Gipson, editors, *Boundary Elements XIII*, pages 875–887, Southampton and Boston, 1991. Computational Mechanics.

[48] J. F. Durodola and R. T. Fenner. Hermitian cubic boundary elements for two dimensional potential problems. *Int. J. Numer. Meth. Engrg.*, 30:1051–1062, 1990.

[49] A. Sáez, R. Gallego, and J. Dominguez. Hypersingular quarter-point boundary elements for crack problems. *Int. J. Numer. Meth. Engrg.*, 38(10):1681–1701, 1995.

[50] S. Selcuk, D. S. Hurd, S. L. Crouch, and W.W. Gerberich. Prediction of interfacial crack path: a direct boundary integral approach and experimental study. *Int. J. Fracture*, 67(1):1–20, 1994.

[51] L. J. Gray and C. San Soucie. Hermite interpolation algorithm for hypersingular boundary integrals. *Int. J. Numer. Meth. Engrg.*, 36:2357–2367, 1993.

[52] B. K. Char, K. O. Geddes, G. H. Gonnet, and S. M. Watt. *Maple User's Guide*. WATCOM Publications Ltd., University of Waterloo, Waterloo, Canada, 1985.

[53] C. Balakrishna, L. J. Gray, and J. H. Kane. Efficient analytical integration of symmetric Galerkin boundary integrals over curved elements; elasticity formulation. *Comput. Methods Appl. Mech. Engrg.*, 117:157–179, 1994.

[54] H. Okada, H. Rajiyah, and S. N. Atluri. A novel displacement gradient boundary element method for elastic stress analysis with high accuracy. *Transactions of the ASME*, 55:786–794, 1988.

[55] L. J. Gray, D. Maroudas, and M. Enmark. Galerkin boundary integral method for evaluating surface derivatives. *SIAM J. Sci. Stat. Comput.* submitted.

[56] L. J. Gray and E. D. Lutz. On the treatment of corners in the boundary element method. *J. Comp. Appl. Math.*, 32:369–386, 1990.

[57] L. J. Gray. A note on Overhauser elements. *Boundary Element Communications*, 5:62–65, 1994.

[58] E. D. Lutz. *Singular and nearly singular integrals.* PhD thesis, Cornell University, 1991.

[59] J. S. Bullock, G. E. Giles, and L. J. Gray. Simulation of an electrochemical plating process. In C. A. Brebbia, editor, *Topics in boundary element research*, volume 7, chapter 7, pages 121–141. Springer Verlag, Berlin and New York, 1990.

[60] V. Sladek, J. Sladek, and M. Tanaka. Regularization of hypersingular and nearly singular integrals in the potential theory and elasticity. *Int. J. Numer. Meth. Engrg.*, 36:1609–1628, 1993.

[61] M. Bonnet. Regularized direct and indirect symmetric variational BIE formulations for three-dimensional elasticity. submitted.

[62] A. Frangi and G. Novati. Symmetric BE method in two-dimensional elasticity: evaluation of double integrals for curved elements. *Computational Mechanics*, 19:58–68, 1996.

[63] S. Sirtori, G. Maier, G. Novati, and S. Miccoli. A Galerkin symmetric boundary element method in elasticity: formulation and implmentation. *Int. J. Numer. Meth. Engrg.*, 35:255–282, 1992.

[64] J. Kane and C. Balakrishna. Symmetric Galerkin boundary formulations employing curved elements. *Int. J. Numer. Meth. Engrg.*, 36:2157–2187, 1993.

[65] A. Aimi, A. Carini, and M. Diligenti. Application of the h-p version of symmetric boundary element method. In *Proceedings of the XII AIMETA Congress: Mechanics of Structures*, volume 1, pages 31–36, 1995.

[66] S. M. Hölzer. The Symmetric Galerkin BEM in elasticity: FEM/BEM coupling, integration and adaptivity. *Computational Mechanics*. submitted.

[67] F. A. de Paula and J. C. F. Telles. A comparison between point collocation and Galerkin for stiffness matrices obtained by boundary elements. *Engineering Analysis with Boundary Elements*, 6(3):123–128, 1989.

[68] L. J. Gray. Symbolic computation of hypersingular boundary integrals. In J. H. Kane, G. Maier, N. Tosaka, and S. N. Atluri, editors, *Advances in boundary element techniques*, pages 157–172. Springer-Verlag, Berlin Heidelberg, 1993.

[69] L. J. Gray. Evaluation of 3D Galerkin singular boundary integrals. in preparation.

[70] F. J. Rizzo, D. J. Shippy, and M. Rezayat. A boundary integral equation method for radiation and scattering of elastic waves in three dimensions. *Int. J. Numer. Meth. Engrg.*, 21:115–129, 1985.

[71] E. D. Lutz and L. J. Gray. Exact evaluation of singular boundary integrals without CPV. *Comm. Num. Meth. Engrg.*, 9:909–915, 1993.

[72] L. J. Gray and G. H. Paulino. Crack tip interpolation, revisited. *SIAM J. Applied Matematics*. (in press).

[73] L. J. Gray and G. H. Paulino. Symmetric Galerkin boundary integral formulation for interface and multi-zone problems. *Int. J. Numer. Meth. Engrg.* in press.

[74] J. Hadamard. *Lectures on Cauchy's Problem in Linear Partial Differential Equations*. Dover Publications, 1952.

[75] N. I. Ioakimidis. Exact expression for a two-dimensional finite part integral appearing during the numerical solution of crack problems in three-dimensional elasticity. *Comm. Appl. Numer. Methods*, 1:183–189, 1985.

[76] A. C. Kaya and F. Erdogan. On the solution of integral equations with strongly singular kernels. *Quart. Appl. Math.*, 45:105–122, 1987.

[77] L. J. Gray and G. H. Paulino. Symmetric Galerkin boundary integral fracture analysis for plane orthotropic elasticity. *Computational Mechanics*. (in press).

[78] F. J. Rizzo and D. J. Shippy. A method for stress determination in plane anisotropic elastic bodies. *Journal of Composite Materials*, 4:36–61, 1970.

[79] A. E. Green. A note on stress systems in aeolotropic materials. *Philosophical Magazine*, 34:416–418, 1943.

[80] K. R. Ghandi. Analysis of an inclined crack centrally place in an orthotropic rectangular plate. *Journal of Strain Analysis*, 7:157–162, 1972.

[81] S. G. Lekhnitskii. *Theory of Elasticity of an Anisotropic Body*. Mir Publishers, Moscow, 1977. English translation 1981.

[82] P. A. Wawrzynek. *Discrete Modeling of Crack Propagation: Theoretical Aspects and Implementation Issues in Two and Three Dimensions*. PhD thesis, Cornell University, Ithaca, NY, 1991.

[83] M. H. Aliabadi, W. S. Hall, and T. G. Phemister. Taylor expansions for singular kernels in the boundary element method. *Int. J. Numer. Meth. Engrg.*, 21:2221–2236, 1985.

[84] Bernard Danloy. Numerical construction of gaussian quadrature formulas for $\int_0^1 (-\log x)\, x^\alpha f(x)\, dx$ and $\int_0^\infty e_m(x) f(x)\, dx$. *Mathematics of Computation*, 27:861–869, 1973.

[85] L. J. Gray and S. J. Chang. Hypersingular formulation for 2D elastic wave scattering. *Engrg. Analy. Boundary Elem.*, 10(4):337–344, 1992.

[86] W. S. Hall and W. H. Robertson. Advanced boundary element calculations for elastic wave scattering. In M. F. McCarthy and M. A. Hayes, editors, *Elastic Wave Propagation*, pages 459–464. Elsevier Science Publishers B. V., 1989.

[87] F. W. J. Oliver. Bessel functions of integer order. In M. Abromowitz and I. E. Steegun, editors, *Handbook of mathematical functions*, chapter 9, pages 355–434. National Bureau of Standards, Washington, D.C., 1972.

[88] T. A. Cruse and W. Van Buren. Three-dimensional elastic stress analysis of a fracture specimen with an edge crack. *International Journal of Fracture Mechanics*, 7:1–15, 1971.

[89] F. J. Rizzo and D. J. Shippy. A formulation and solution procedure for the general non-homogeneous elastic inclusion problem. *Int. J. Solids Struct.*, 4:1161–1173, 1968.

[90] V. Sladek and J. Sladek. Improved computation of stresses using the boundary element method. *Appl. Math. Modelling*, 10:249–255, 1986.

[91] J. Hildenbrand and G. Kuhn. Numerical computation of hypersingular integrals and application to the boundary integral equation for the stress tensor. *Engineering Analysis with Boundary Elements*, 10:209–217, 1992.

[92] C. Fiedler. On the calculation of boundary stresses with the Somigliana identity. *Int. J. Numer. Meth. Engrg.*, 38:3275–3295, 1995.

[93] M. Guiggiani. Hypersingular integral equations and superaccurate stress evaluation. In C. A. Brebbia and J. J. Rencis, editors, *Boundary Elements XV*, volume 1, pages 413–428, Southampton and Boston, 1993. Computational Mechanics Publications.

[94] E. D. Lutz, L. J. Gray, and A. R. Ingraffea. Indirect evaluation of surface stress in the boundary element method. In L. Morino and R. Piva, editors, *Boundary Integral Methods: Theory and Applications. Proc. IABEM Symposium*, Berlin, 1990. Springer Verlag.

[95] Z. Zhao. On the calculation of boundary stresses in boundary elements. *Engrg. Analy. Boundary Elem.*, 16(4):317–322, 1997.

[96] H. Okada, H. Rajiyah, and S. N. Atluri. Non-hypersingular integral representations for velocity (displacement) gradients in elastic/plastic solids (small or finite deformations). *Computational Mechanics*, 4:165–175, 1989.

[97] T. Matsumoto, M. Tanaka, and H. Hirata. Boundary stress calculation using regularized boundary integral equation for displacement gradients. *Int. J. Numer. Meth. Engrg.*, 36:783–797, 1993.

[98] L. J. Gray and L. L. Manne. Hypersingular boundary integrals at a corner. *Engrg. Analy. Boundary Elem.*, 11:327–334, 1993.

[99] A. F. Bower and L. B. Freund. Finite element analysis of electromigration and stress induced diffusion in deformable solids. In A. S. Oates, W. F. Filter, R. Rosenberg, A. L. Greer, and K. Gadepally, editors, *Materials Reliability in Microelectronics V*, volume 391 of *Materials Research Society Symposia Proceedings*, pages 177–188, Pittsburgh, 1995. Materials Research Society.

[100] D. Maroudas. Dynamics of transgranular voids in metallic thin films under electromigration conditions. *Appl. Phys. Lett.*, 67:798–800, 1995.

[101] D. Maroudas and S. T. Pantelides. Theory and computer simulation of grain boundary and void dynamics in polycrystalline conductors. In A. S. Oates, W. F. Filter, R. Rosenberg, A. L. Greer, and K. Gadepally, editors, *Materials Reliability in Microelectronics V*, volume 391 of *Materials Research Society Symposia Proceedings*, pages 151–162, Pittsburgh, 1995. Materials Research Society.

[102] D. Maroudas, M. N. Enmark, C. M. Leibig, and S. T. Pantelides. Analysis of damage formation and propagation in metallic thin films under the action of thermal stresses and electric fields. *Journal of Computer-Aided Materials Design*, 2:231–258, 1995.

[103] D. Maroudas, M. Enmark, L. J. Gray, and E. F. D'Azevedo. Morphological stability and dynamics of voids in metallic thin-film interconnects under electromigration conditions. in preparation.